이학박사 학위논문

CPNE7-Induced Autophagy in Mature Odontoblast and Epithelial-Mesenchymal Interaction in Alveolar Bone

성숙한 상아모세포에서 CPNE7 유도-자가포식과 치조골에서 상피간엽상호작용

2021 년 8 월

서울대학교 대학원

치의과학과 세포 및 발생생물학 전공

손 철

CPNE7-induced autophagy in mature odontoblast and epithelial-mesenchymal interaction in alveolar bone

지도교수 박 주 철

이 논문을 이학박사 학위논문으로 제출함
2021 년 7 월

서울대학교 대학원
치의과학과 세포 및 발생생물학 전공
손 철

손철의 박사학위논문을 인준함
2021 년 7 월

위 원 장 류 현 모

부위원장 박 주 철

위 원 이 승 복

위 원 조 의 식

위 원 강 찬 희

CPNE7-induced autophagy in mature odontoblast and epithelial-mesenchymal interaction in alveolar bone

By

Chul Son

Advisor:

Prof. Joo-Cheol Park, D.D.S., ph.D.

A thesis submitted fulfillment of the requirement for the degree of Doctor of philosophy in Seoul National University

July, 2020

Professor	Hyun-Mo Ryoo
Professor	Joo-Cheol Park
Professor	Seung-bok Lee
Professor	Eui-Sic Cho
Professor	Chanhee Kang

ABSTRACT

CPNE7-Induced Autophagy in Mature Odontoblast and Epithelial-Mesenchymal Interaction in Alveolar Bone

Son, Chul

Department of Oral Histology-Developmental Biology

School of Dentistry

The Graduate School

Seoul National University

(Directed by prof. Joo-Cheol Park, Ph.D.)

Tooth and periodontal development are modulated by reciprocal and sequential interaction between dental mesenchyme and epithelium, an epithelial-mesenchymal interaction (EMI). EMI includes various factors such as Copine-7 (CPNE7) and Bone morphogenetic protein 4 (BMP4). CPNE7 is known to play an essential role in odontoblast differentiation and tubular dentin formation. BMP4 is known to play an important role in limb patterning and skeletogenesis. However, the underlying mechanisms of CPNE7 on physiological dentin regeneration and different responsiveness of alveolar bone and long bone by BMP4 have not yet been elucidated.

Odontoblasts, long-lived post-mitotic cells, can live for decades in the

organism and exhibit a distinct type of cellular aging characterized by a progressive functional decline. Consequently, restoring the function of mature or aged odontoblasts in the tooth is essential for physiological dentin regeneration; however, no molecule regulating the cellular activity of mature odontoblasts has yet been identified. I suggest that CPNE7 can reactivate the function of mature odontoblasts by inducing autophagy. CPNE7 elevated expression of widely used autophagy marker, microtubule-associated protein light chain 3 (LC3 II), and autophagosome formation in pre-odontoblasts and mature odontoblasts. Dentin mineralization markers, DSP and DMP-1, and dentin formation capacity were increased in recombinant CPNE7-treated mature odontoblasts by CPNE7-induced autophagy. Also, odontoblast process markers, NESTIN and TAU, expression were elevated, and morphology of mature odontoblast process was identical as physiological odontoblast process when autophagy was induced by CPNE7. Furthermore, CPNE7 eliminated lipofuscin, the aging pigment which obstructs cellular function and gives off toxicity, in mature odontoblasts by inducing autophagy. These phenomena were also identical *in vivo* mouse indirect pulp capping model with physiological dentin regeneration. Even though rapamycin, the most renowned activator of autophagy, also elevated autophagy in pre-odontoblasts and mature odontoblasts, its reactivation capacity on mature odontoblasts was insufficient compared to CPNE7. In short, these results suggest that CPNE7 restores the capacity of dentin formation, odontoblast process elongation, and removal of lipofuscin in mature odontoblasts by inducing autophagy in some other way of rapamycin.

Alveolar bone plays a crucial role in maintaining tooth and periodontium

structure by repositioning the tooth in the direction of the stimulus. It has distinct characteristics to other bones such as sensitivity to external mechanical or pharmacological stimuli. Especially, long bone and alveolar bone have fundamental differences. They are derived from the different developmental origin, lateral plate and neural crest (NC), respectively and experience different epithelial-mesenchymal interaction (EMI) during development. For these reasons, I suggest that these fundamental differences can make distinct responsiveness of alveolar bone and long bone. For the research, I harvested primary mouse bone derived-cells from the alveolar and long bone. Although mouse alveolar bone derived-cells (mABDCs) and mouse long bone derived-cells (mLBDCs) exhibited some similar properties like morphology and proliferation rates, both showed distinct expression of NC and EMI-related genes and mineralization capacity. Moreover, transcriptome profiles showed disparate patterns, notably on osteogenic, NC, and EMI-related genes. Expression patterns of most of these genes were distinguishable during osteogenic differentiation. Among the EMI-related proteins, BMP4 elevated the expression of several osteogenic genes, Msx2, Dlx5, and Bmp2, more noticeably in mABDCs than in mLBDCs. These patterns were more obviously verified during osteogenic differentiation. Furthermore, BMP4-treated mABDC showed massive alveolar bone formation *in vivo* ectopic transplantation as opposed to its counterpart. The finding of the present study provides a glimpse of different responsiveness to EMI by distinct gene regulation of alveolar bone and long bone.

Collectively, these studies provide the underlying mechanism of CPNE7 regenerating physiological dentin through reactivation of mature odontoblasts and an EMI-related factor, BMP4, which has critical bone formation effects on alveolar

bone. Together, they also introduce the potential of CPNE7 and BMP4 as dentinal and alveolar bone loss-targeted clinical applications respectively.

Keywords: epithelial-mesenchymal interaction, copine-7, BMP4, autophagy, reactivation, responsiveness

Student Number: 2015-22088

CONTENTS

LIST OF TABLES AND FIGURES

CHAPTER I. GENERAL INTRODUCTION

1. Odontoblast

Odontoblasts are specialized cells responsible for the formation of the physiological dentin, the largest mineralized tissue in the tooth. Physiological odontoblasts have several distinct characteristics to other cells in dental pulp (Bleicher, 2014)

During the differentiation, odontoblasts acquire a specific morphology with a long cellular process called the odontoblast process. They mainly secrete mineralized dentin matrix at the process in the pre-dentin region and move backward, leaving their newly formed cellular process. These developmental processes of odontoblasts make physiological dentin as tubular dentin (Weinstock and Leblond, 1974). Some tooth restoration materials are known to promote the formation of tertiary dentin with tubeless structure beneath the tooth defect site. However, the tubeless structure entrapping cells has more limitations than the tubular structure. First of all, due to a lack of osteocyte canaliculi-like structure, entrapped cells eventually die and form empty space causing diminishment in the hardness of tertiary dentin. Also, unlike the tubular dentin with the odontoblast process, the structure without tubule and odontoblast process cannot immediately respond to the external stimuli while sensing bacterial infection and rapid immune response of physiological odontoblast at the early stage is crucial for maintaining the vitality of pulp tissue. However, it is hard to find the method inducing tubular dentin structure formation or regeneration (Kim, 2017).

Odontoblasts are long-lived post-mitotic cells. Dental mesenchymal cells undergo mitosis at the early developmental stage and are sequentially changed depend on the functional stage through odontogenic differentiation and aging (Couve, 1986). They are getting larger and longer with increased secretory machinery during the pre-odontoblast to secretory odontoblast phase. On the contrary, odontoblasts shrink with decreased intracellular organelles for their survival during the transitional to aged odontoblasts stage. Some age-related pigments like lipofuscin progressively accumulate, transitioning from mature to aged odontoblast. These phenomenon change debilitated cellular function and responsiveness of aged odontoblasts (Couve et al., 2013). Therefore, functional restoration of mature or aged odontoblasts is essential for the regeneration of the physiological dentin-pulp complex.

2. Autophagy

The autophagic-lysosomal system consists of lysosome mediated self-digestive pathways by which cells regulate the turnover of long-lived proteins and organelles to maintain cellular homeostasis (Couve et al., 2013). There are three types of autophagy: macroautophagy, microautophagy, and chaperone-mediated autophagy, and the term “autophagy” usually indicates macroautophagy unless specified (Mizushima, 2007). Autophagy is a process of cellular self-cannibalism in which portions of the cytoplasm are sequestered within double- or multi-membraned vesicles and then delivered to lysosomes for bulk degradation (Rubinsztein et al., 2011). The most renowned key regulator of autophagy is the mechanistic target of rapamycin (mTOR). The activity of mTOR is inhibited under

nutrient starvation, a well-known crucial step for autophagy induction in eukaryotes. Rapamycin, a notable autophagy inducer, promotes autophagy by inhibiting the phosphorylation of mTOR (Scott et al., 2004). As of now, the function of autophagy is known as the housekeeping process under conditions induced by various stresses like starvation. The physiological role of autophagy during the development and differentiation in tooth come to the fore (Yang et al., 2013; Park et al., 2020). The effect of autophagy modulation in mature and aged odontoblasts has not yet been elucidated.

Lipofuscin, an aging pigment, is also a derivative of mitophagy. The constitutive turnover of mitochondrial components via autophagy causes the progressive accumulation of lipofuscin deposits within autolysosomes. These deposits are considered inherently toxic and could affect cell function by inhibiting lysosomal-degradative capacities (Terman et al., 2010). However, there is a limited approach to the elimination of lipofuscin in long-lived post-mitotic cells.

3. Epithelial-mesenchymal interaction (EMI)

Interactions between epithelium and mesenchyme are common features of different organs' morphogenesis at the early stages. In some of these interactions, the epithelium can induce differentiation of the mesenchyme vice versa, and play an instructive role mediated by differential activation of genes in responding cells (Ribatti and Santoiemma, 2014).

The reciprocal and sequential interaction between dental mesenchyme and epithelium constitutes the core of the molecular program. The interactions are

mediated by the conserved signal molecules activating the expression of specific transcription factors, which in turn regulate the expression of numerous other genes important for advancing morphogenesis and cell differentiation in the developing tooth (Nanci, 2017). Despite the progressive comprehension on the molecular basis of tooth development and differentiation, little is known about molecules involving epithelial-mesenchymal interaction (EMI).

The role of EMI in periodontium development is less established than in tooth development. The dental epithelium-derived Hertwig epithelial root sheath (HERS) and epithelial cell rests of Malassez (ERM) take an essential role in periodontium development and homeostasis (Bosshardt et al., 2015). However, the precise molecular mechanism of EMI is not well understood. Therefore, progressive studies of EMI in tooth and periodontium development are needed.

4. Copine-7 (CPNE7)

During tooth development, numerous signaling molecules and transcription factors mediate odontoblast differentiation and dentin formation through sequential EMI. Especially, early odontogenic differentiation of ectomesenchymal cells at dental papilla was induced by adjacent inner dental epithelium cells. Based on this concept, secretion was collected from mouse apical bud cells that can differentiate into ameloblasts. This preameloblast-conditioned medium (PA-CM) showed odontogenic differentiation and dentin formation of human dental pulp cells (hDPCs). Among these factors in PA-CM, CPNE7 protein was identified as the candidate of odontogenic differentiation inducer (Lee et al., 2011b). Further

researches elucidated the effects of CPNE7, which regulates the differentiation of mesenchymal cells into odontoblasts, through molecular mechanism regulating expression of Dspp, typical odontoblast marker, via nucleolin (Oh et al., 2015; Seo et al., 2017). In distinction to hDPCs, the indirect pulp capping canine model showed CPNE7 stimulates reactionary dentin and peritubular dentin formation (Choung et al., 2016). On the other hand, the molecular mechanism of physiological dentin regeneration through CPNE7 is still elusive.

5. Alveolar bone

Periodontium supports and adjusts the tooth, which received various external stimuli. The alveolar bone is one of the periodontal tissue covering tooth roots. Alveolar bone remodeling plays an important role in maintaining tooth and periodontium by repositioning the tooth in the direction of the stimulus (Cho and Garant, 2000; Sodek and McKee, 2000). Periodontitis, one of the most frequent disease for adults, cause alveolar bone loss respect to progression of the disease, and condition of alveolar bone is important for supporting the dental implant (Papapanou et al., 2018; Greenwell et al., 2019). Although the significance of alveolar bone and its regeneration increases, there is still a great gap to be filled in through further investigation.

Alveolar bone has different characteristics from other bones. Because alveolar bone responds sensitively to external stimuli, its remodeling occurs easily and its loss happens rapidly when without stimulus (Sodek and McKee, 2000; Metzger et al., 2017). Some of the osteoporosis drugs cause critical bone necrosis on the jaw

bone, including alveolar bone, while they have positive effects on other bones (Rosella et al., 2016; Nicolatou-Galitis et al., 2019). The reason behind the distinct response of alveolar bone needs to be clarified.

Two developmental differences exist between long bone and alveolar bone; developmental origin and EMI during development are different (Lumsden, 1988; Zeller et al., 2009). Furthermore, recent studies give a clue that ERM, epithelial cells remaining in the mature periodontal ligament, could play a role in alveolar bone remodeling in adults (Silva et al., 2017). The distinct feature of two kinds of bones could be derived from different crosstalk of EMI.

6. Rationale and outline of the thesis experiments

A key purpose of this thesis is to investigate the underlying mechanism of CPNE7 on mature odontoblast reactivation via autophagy induction, and the possible roles of EMI in alveolar bone characteristics and regeneration. To examine these objectives, I investigated the effect of CPNE7 in the beagle and mouse indirect pulp capping model. Western blot, immunocytochemistry, optical, confocal microscopy, and transmission electron microscopy analysis were performed to investigate the autophagy, protein expression, lipofuscin levels, and odontoblast process elongation in response to CPNE7. Odontoblast differentiation and dentin formation with respect to CPNE7 was analyzed with alizarin red S staining and ectopic transplantation *in vivo*. In a similar manner, how EMI is involved in the development and differentiation of alveolar bone in mouse bone-derived cells was also explored. I additionally examined whether BMP4, EMI-

related factor, is required for alveolar bone formation through ectopic transplantation *in vivo*.

CHAPTER II.

CPNE7-Induced Autophagy Restores the Physiological Function of Mature Odontoblasts

*** This chapter has been largely reproduced from an article published by Park YH, Son C, and Park JC. (2021). Front Cell Dev Biol., 9:655498**

I. ABSTRACT

Dentin, which composes most of the tooth structure, is formed by odontoblasts, long-lived post-mitotic cells maintained throughout the entire life of the tooth. In mature odontoblasts, however, cellular activity is significantly weakened. Therefore, it is important to augment the cellular activity of mature odontoblasts to regenerate physiological dentin; however, no molecule regulating the cellular activity of mature odontoblasts has yet been identified. Here, I suggest that Copine-7 (CPNE7) can reactivate the lost functions of mature odontoblasts by inducing autophagy.

CPNE7 was observed to elevate the expression of microtubule-associated protein light chain 3-II (LC3-II), an autophagy marker, and autophagosome formation in the pre-odontoblast and mature odontoblast stages of human dental pulp cells. CPNE7-induced autophagy upregulated DSP and DMP-1, odontoblast differentiation and mineralization markers, and augmented dentin formation in mature odontoblasts. Furthermore, CPNE7 also upregulated NESTIN and TAU, which are expressed in the physiological odontoblast process, and stimulated the elongation of the odontoblast process by inducing autophagy. Moreover, lipofuscin, which progressively accumulates in long-lived post-mitotic cells and hinders their proper functions, was observed to be removed in recombinant CPNE7-treated mature odontoblasts. Thus, CPNE7-induced autophagy reactivated the function of mature odontoblasts and promoted the formation of physiological dentin *in vivo*. On the other hand, the well-known autophagy inducer, rapamycin, promoted odontoblast differentiation in pre-odontoblasts but did not properly reactivate the function of mature odontoblasts.

These findings provide evidence that CPNE7 functionally reactivates mature odontoblasts and introduce its potential for dentinal loss-targeted clinical applications.

II. INTRODUCTION

Teeth are hard, mineral-rich structures that serve to masticate food. (Brudevold et al., 1960). Teeth also serve as a mineralized outer barrier that protect the inner dental pulp from external stimuli and damage (Craig and Peyton, 1958). Dentin makes up more than 70% of the entire tooth structure, and it forms a bridge between the dental pulp and the enamel through a dentinal tubule structure (Marshall, 1993). Some animals can replace their teeth throughout their lives (van Nievelt and Smith, 2005). However, humans have only two sets of teeth: deciduous teeth, which generally loosen and fall out prior to adulthood, and permanent teeth, which replace the deciduous teeth and stay in place for the remaining lifespan (Kim et al., 2014). Thus, severe injury to the permanent teeth is irreversible and results in extraction since dentin forming odontoblasts cannot be normally replaced in humans.

Odontoblasts are ectomesenchyme-derived post-mitotic cells that form a significant layer in the dentin-pulp complex. As they differentiate from the dental mesenchyme (pre-odontoblasts), odontoblasts become highly polarized and form a cytoplasmic elongation called the odontoblast process. Leaving their processes in the dentinal tubules, odontoblasts (secretory odontoblasts) retreat from the dentin and actively secrete organic dentin matrix that is then progressively mineralized (Couve, 1986). However, when physiologic dentin is completed, active secretory odontoblasts gradually transform into a terminally differentiated stage (mature odontoblasts) with debilitated cellular function and responsiveness. Mature odontoblast’s longevity is sustained by elaborate autophagic activity that regulates organelle and protein renewal. However, progressive dysfunction of that system

can debilitate the activity of mature odontoblasts and eventually impair their dentin maintenance capacity (Couve et al., 2013).

Copine-7 (CPNE7), a dental epithelium-derived factor, has been reported to promote odontogenic differentiation and physiological dentin formation (Oh et al., 2015). This secreted factor from the pre-ameloblasts, binds to nucleolin on the cell surface of pre-odontoblasts and translocates to the nucleus, where it regulates dentin sialophosphoprotein (Dspp) expression (Seo et al., 2017; Park et al., 2019). Of the numerous odontoblast differentiation-promoting factors reported so far, non-collagenous dentin matrix proteins (Duque et al., 2006; Kim, 2017) and CPNE7 (Choung et al., 2016; Lee et al., 2020) have been shown to form the physiological tubular dentin that contains the dentinal tubules that hold the odontoblast processes. However, the precise mechanism of CPNE7-mediated physiologic tubular dentin regeneration in adult dentin has not yet been elucidated. In the process of CPNE7-mediated physiological dentin regeneration, CPNE7 could augment the functional quality of mature odontoblasts and promote the elongation of their cellular processes into newly formed dentinal tubules via cellular remodeling. Considering the connections between microtubules, which contribute to odontoblast processes (Nishikawa and Kitamura, 1987), and autophagy, along with autophagy defect leading to impaired dentin (Park et al., 2020), the effects suggest a possible correlation between CPNE7 and autophagy in mature odontoblast and their potential to restore the cell's functional and physiological activity.

In this study, I identify the association between CPNE7 and autophagy in mature odontoblasts and its effect in functional restoring. I hypothesized that CPNE7 may be connected with autophagy-mediated odontoblast process

elongation and physiological dentin formation. Specifically, I aimed to evaluate (1) the involvement of autophagy in CPNE7-mediated odontoblast process elongation and mineralization *in vitro*, (2) the ramifications of CPNE7 in calcified tissue formation using subcutaneous transplantation *ex vivo*, and (3) the possible application of CPNE7-mediated physiological dentin formation using a mouse dentin exposure model *in vivo*.

III. MATERIALS AND METHODS

Indirect Pulp Capping Model with Canine Teeth

All experiments using beagles were conducted under the guidelines provided by the Institutional Animal Care and Use Committee of Seoul National University (SNU-171020-5-2). The indirect pulp capping was performed as described previously (Lee et al., 2020). Three beagle dogs (aged 1-2 y) were examined throughout the experiment. Each group consisted of 2 premolars per animal, totaling 6 premolars. Briefly, after class V cavity preparation, cavities were either untreated or treated with a topical application of rCPNE7 protein (1 μg per tooth). The animals were sacrificed after 4 weeks of post-operation. The experimented beagle teeth were fixed at 4% PFA for 24 hours. After fixation, the experimented teeth were decalcified in 10% formic acid (Georgia Chem, 64-18-6) over a month. For histological analysis, the decalcified tissue were embedded in paraffin. 5-μm serial sections were mounted on silanized slides and stored in air-tight cases at 4 °C. For the histomorphometric analysis, samples were analyzed with H&E staining.

Cell Culture

The experimental protocol for this study was approved by the Institutional Review Board (S-D20140007). All methods were performed in accordance with the relevant guidelines and regulations. Informed consent was obtained from all participants. Impacted human third molars were collected from the Seoul National

University Dental Hospital (Seoul, Republic of Korea). The human whole pulp cell isolation was executed as described previously (Jung et al., 2011). hDPCs were cultured in minimum essential medium α (Gibco BRL, 12571063) supplemented with 10% heat-inactivated fetal bovine serum (FBS; Gibco BRL, 16000044) and antibiotic-antimycotic (Gibco BRL, 15240062) at 37 ℃ in an atmosphere with 5% CO2. To induce the hDPCs into odontogenic differentiation, 80-90% confluent cells were cultured with 5% FBS, ascorbic acid (50 μg/㎖; VWR, 0143), and β-glycerophosphate (10 mM; Sigma-Aldrich, G9422) for up to 21 days. The cells were then treated with recombinant CPNE7 (rCPNE7, 100 ng/ml; Origene, TP306428), 3-methyladenine (3-MA, 5 mM; Sigma-Aldrich, M9281), or rapamycin (100 nM; Sigma-Aldrich, R8781) for 24 h and harvested. For the cell morphological analysis, differentiated and undifferentiated hDPCs were seeded into 35 mm confocal dishes (SPL, 101350) at a density of 1 × 103 cells per dish. The cells were then treated with rCPNE7, 3-MA, or rapamycin for 7 days. An optical microscope (Olympus Co., CKX41) connected to a computer and charge-coupled device camera (IMT i-solution Inc., IMTcamCCD Pro2) was used to take images of the samples.

Western Blot Analysis

Western blotting was performed as previously described (Seo et al., 2017). Affinity-purified rabbit polyclonal anti-CPNE7 and anti-DSP antibodies were produced as previously described (Lee et al., 2010; Lee et al., 2011b). Anti-LC3 B polyclonal antibody (Abcam, ab48394), anti-TAU monoclonal antibody (TAU-5;

Thermo Fisher Scientific, AHB0042), anti-phospho-mTOR [Ser2448] (mechanistic target of rapamycin kinase) polyclonal antibody (Cell Signaling Technology, 5536), anti-DMP-1 (dentin matrix protein 1) polyclonal antibody (Abcam, ab103203), anti-NESTIN monoclonal antibody (10C2; Thermo Fisher Scientific, MA1-110), and anti-GAPDH monoclonal antibody (GA1R; Thermo Fisher Scientific, MA5-15738) were purchased from the respective companies. Protein loading was assessed by the expression of GAPDH. All reactions were performed in triplicate. Semi-quantitative analysis were performed using ImageJ software (National Institute of Health).

Immunocytochemistry and Immunofluorescence

hDPCs fixed in 4% paraformaldehyde (PFA; T&I, BFA-9020) and deparaffinized tissue sections were treated with phosphate-buffered saline (PBS) containing 0.5% Triton X-100 (Amresco, 0694) for permeabilization. After being washed and blocked, the cells were incubated for 1 h with LC3B antibody (1:100) or α-TUBULIN (1:100, YOL1/34; Santa Cruz Biotechnology, sc-53030) antibody and TAU antibody (1:50) in blocking buffer (PBS and 2% bovine serum albumin (BSA; Gibco BRL, 30063-572)). Tissue sections were incubated with α-TUBULIN antibody (1:200) overnight at 4 ℃. Subsequently, fluorescein isothiocyanate (FITC)-conjugated goat anti-rabbit IgG antibody (1:200; Thermo Fisher Scientific, F2765), Alexa Fluor 488-conjugated goat anti-rat IgG antibody (1:200; Thermo Fisher Scientific, A11006), or Cy3-conjugated goat anti-mouse IgG antibody (1:200; Merck Millipore, AP124C) was applied. After being washed, the

chromosomal DNA in the nucleus was stained with 4′,6-diamidino-2-phenylindole (DAPI) during the mounting procedure (Vector Labs, H-5000). Samples were visualized using confocal laser scanning microscopy (Carl Zeiss, LSM 800).

TEM Analysis

Cells were harvested with trypsin and ethylenediaminetetraacetic acid (EDTA) and fixed with 2.5% glutaraldehyde (GA; Sigma-Aldrich, G7651) in PBS. They were then post-fixed in buffered 1% osmium tetroxide, embedded and fixed a second time in 2.5% GA, cut into 1 mm sections, and dehydrated through a graded ethanol series and propylene oxide prior to microwave infiltration of 1:1 Spurr/Epon resin. The polymerized blocks were sectioned on an ultramicrotome (Leica, EM UC6), and 70-nm sections were re-mounted on 100-mesh grids and stained with uranyl acetate and Reynolds lead citrate. Images were acquired with a JEM-1400 Flash (JEOL).

Alizarin Red S Staining for Mineralized Matrix

hDPCs were cultured with an odontogenic induction medium for 21 days. On day 21, the cells were seeded into 35 mm culture dishes at a density of 1 × 105 cells per dish. The cells were then treated with rCPNE7, 3-MA, rCPNE7+3-MA, or rapamycin and cultured in odontogenic induction medium for 7 more days. After 7 days, cells were fixed with 4% PFA overnight at 4 ℃ and stained with 40 mM alizarin red S (Sigma-Aldrich, A5533), pH 4.2, for 30 min at room temperature. To

quantify the mineralized matrix in culture, alizarin red S stain was eluted using 0.5 mL of 5% sodium dodecyl sulfate (Amresco, 0227) in 0.5 N HCl solution and shaken for 30 min; the absorbance of the eluted dye was measured at 405 nm.

Ectopic Transplantation *in vivo* and Histological Analysis

Primary cultured hDPCs were differentiated for 21 days *in vitro*. Differentiated cells (2 × 106) were mixed with 100 mg of hydroxyapatite/tricalcium phosphate (HA/TCP) ceramic powder (Zimmer Biomet, 00110900612) alone or with either rCPNE7 (1 μg), 3-MA (40 mM), rCPNE7+3-MA, or rapamycin in a 0.5% fibrin gel. The cells were then transplanted subcutaneously into immunocompromised mice (NIH-bg- nu-xid; Harlan Laboratories) for 6 weeks. For the histomorphometric analysis of the newly formed mineralized tissue, samples were harvested and fixed in 4% PFA, decalcified in 10% EDTA (pH 7.4; Georgia Chem, ED2041), embedded in paraffin, and stained with hematoxylin and eosin (H&E) and Masson's trichrome (Polysciences Inc, 25088).

H&E and Masson's Trichrome Staining

Tissue sections were deparaffinized in xylene (DUKSAN Chemicals, UN1307) and rehydrated with ethanol (DUKSAN Chemicals, UN1170). For H&E staining, sections were stained with hematoxylin (Vector Labs, H-3401) for 4 min and eosin (T&I, BEY-9005) for 2 min. For Masson's trichrome staining, sections

were stained with Weigert's hematoxylin for 10 min, 1% Biebrich-scarlet-acid fuchsin solution for 20 min, 5% phosphotungstic acid for 10 min, and 2.5% aniline blue solution for 20 min and then differentiated in 1% acetic acid for 1 min.

Lipofuscin Analysis

Lipofuscin accumulation was characterized in tissue sections from coronal odontoblasts and primary cells labeled with DAPI. Lipofuscin deposits were visualized and analyzed under confocal laser scanning microscopy with a 488-nm laser line for excitation.

Mouse Indirect Pulp Capping and Tissue Preparation

All experiments using mice followed protocols approved by the Institutional Animal Care and Use Committee of Seoul National University (SNU-171115-3-6). Fifteen mice (aged 1 M) were used for this experiment. The mice were anesthetized with a 2.5% 2-methyl-2-butanol (Avertin; Sigma, 240486) solution diluted with RNase-free water (T&I, BWA-8000). The oral cavity was opened with a mouth retractor to expose the molars. The maxillary first molars were cleaned with 0.5% chlorhexidine. Then, the center of the first molar was drilled using a carbide bur (FG1/4). The drilling stopped previously to pulp exposure. The cavity treatments were divided into 5 groups: (1) control (PBS+GI), (2) rCPNE7 (rCPNE7+GI), (3) 3-MA (3-MA+GI), (4) rCPNE7 and 3-MA (rCPNE7+3-MA+GI), and (5) rapamycin (rapamycin+GI). The defect areas were

covered with GI cement after the topical treatment appropriate to each group. Each group contained 2 first molars per animal, totaling 6 first molars per group. The animals were sacrificed 4 weeks post-operation. The mouse heads were fixed in 4% PFA in PBS for 24 h at 4 °C. After fixation, the heads were decalcified in 10% EDTA (pH 7.4), embedded in paraffin, and cut for histological analysis. 4-μm serial sections were mounted on silanized slides and stored in air-tight cases at 4 °C. All tissues were sectioned on the frontal plane. For the histomorphometric analysis, samples were analyzed with H&E and Masson's trichrome staining or processed for immunohistochemistry.

Immunohistochemistry

Sections were incubated overnight at 4 °C with rabbit polyclonal LC3B antibody (1:200) in 2% BSA/PBS, pH 7.4. Negative control sections were incubated in 2% BSA/PBS. Sections were then incubated in 2% BSA/PBS mixed with biotin-labeled goat anti-rabbit immunoglobulin G (IgG) (1:200; Vector Labs, BP-9100) as the secondary antibody, washed, and incubated in avidin-biotin-peroxidase complex (Vector Labs, PK-6100). Peroxidase was revealed by incubation with methanol containing 3% H2O2 (JUNSEI, 7722-84-1). Signals were converted using a diaminobenzidine kit (Vector Labs, SK-4100). Nuclei were stained with hematoxylin.

Statistical Analysis

All values are expressed as the mean ± SD of at least three independent experiments. Statistical significance between two groups was determined using Mann-Whitney U test. Differences were considered statistically significant at $*P < 0.05$.

IV. RESULTS

CPNE7 Induces Autophagic Activity in Both Pre-odontoblasts and Mature odontoblasts

Our previous studies showed that CPNE7 induces odontoblastic differentiation of human dental pulp cells (hDPCs) *in vitro* and promotes dentin formation *ex vivo* (Lee et al., 2011b; Oh et al., 2015). Here, I investigated the role of CPNE7 in the mature odontoblasts of beagle dogs. Beagle dog pre-molar defect models were created by exposing the dentinal tubules through drilling. The prepared defects were divided into 2 groups: the non-treated control group and the recombinant human CPNE7 (rCPNE7)-treated group. The exposed dentin of the 2 groups was filled with glass ionomer cement (GI cement) after topical treatment. There was no change in the control group, but tubular dentin containing odontoblast processes was observed at the defect sites of the rCPNE7-treated group (Figure 1A). Those findings suggest that CPNE7 may augment their cellular function and result in physiological tubular dentin regeneration, despite mature odontoblast's low capacity to react to external stimuli.

Next, I tried to define the approximate period when an odontoblast became terminally differentiated, or "mature" *in vitro*. hDPCs were cultured for 21 days in an odontoblast differentiation medium. Afterwards, the expression patterns of CPNE7 and a representative odontoblast differentiation and mineralization marker, dentin sialoprotein (DSP), were analyzed. CPNE7 expression increased from days 0 to 7 (early stage of differentiation) and then progressively decreased until day 21 (late stage of differentiation). DSP showed a similar expression pattern,

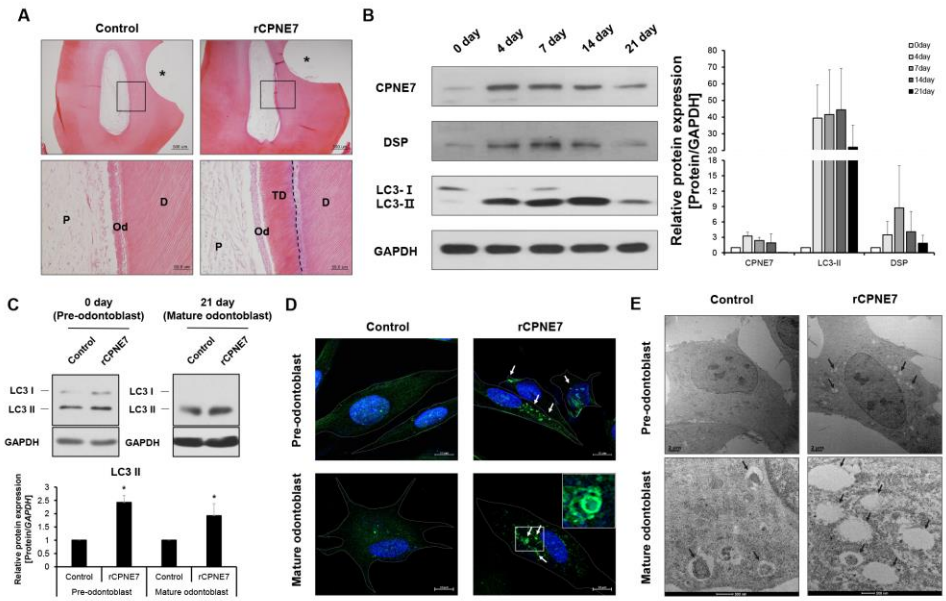

Figure 1. CPNE7 induces autophagic activity in both pre-odontoblasts and mature odontoblasts. (A) Histological analysis of beagle dog pre-molar defect model. Scale bars = 500 mm. The asterisk shows the tooth defect area. Boxed areas are shown at higher magnification. Scale bars = 50 mm. The dotted line shows the boundary of tubular dentin newly formed from native dentin. (B) Western blot analyzing the protein expression patterns of CPNE7, LC3, and DSP in primary human dental pulp cells (hDPCs) during odontogenic differentiation. (C–E) Autophagic activity was analyzed in control and rCPNE7-treated hDPCs at the pre-odontoblast stage (day 0) and the mature odontoblast stage (day 21). (C) LC3 II protein levels were evaluated by western blotting. (D) Representative immunofluorescence images of LC3 (green dot; white arrows). DAPI (blue) counterstaining indicates the nucleus. Scale bars = 10 mm. Boxed areas are shown at higher magnification. (E) Autophagic vacuoles (black arrows) were observed by transmission electron microscopy. Scale bars = 500 nm. hDPCs were treated with

rCPNE7 (100ng/ml) for 24 h. CPNE7, copine-7; rCPNE7, recombinant CPNE7; P, pulp; Od, odontoblast; D, dentin; TD, tubular dentin; LC3, microtubule-associated protein 1A/1B-light chain 3; DSP, dentin sialoprotein. Significant differences are shown with asterisks. *$P < 0.05$.

with its expression significantly weakening around day 21 (Figure 1B). Therefore, I set day 21 as the time at which odontoblasts reached a mature state with debilitated cellular activity and responsiveness.

A previous study demonstrated that autophagy is involved in odontoblast differentiation and tooth morphogenesis during tooth development (Park et al., 2020). To determine whether CPNE7 affects autophagic activity in odontoblasts, I identified changes in the levels of microtubule-associated protein light chain 3-II (LC3-II), a widely used autophagy marker, in rCPNE7-treated hDPCs. Upon the induction of autophagy, a cytosolic form of LC3 (LC3-I) conjugates to phosphatidylethanolamine to form an LC3-phospholipid conjugate (LC3-II), which is localized to autophagosomes and autolysosomes. Therefore, changes in LC3 localization have been used to measure autophagy (Tanida et al., 2004; 2008). Interestingly, LC3-II showed similar expression patterns to CPNE7 in differentiating hDPCs: increased expression in the pre-odontoblast state and decreased expression in the mature odontoblast state (Figure 1B). In both the pre-odontoblast and mature odontoblast states, LC3-II was significantly upregulated in the CPNE7-treated group compared to the control (Figure 1C). Immunofluorescence testing of LC3 showed only a few autophagic vacuoles in the control group, whereas many more were detected in the rCPNE7-treated cells (Figure 1D). I used transmission electron microscopy (TEM) to detect the presence of any ultrastructural differences in cells between the control and rCPNE7-treated groups. Consistently, more autophagic vacuoles were detected in cells in the rCPNE7-treated group than in the control (Figure 1E). Those results suggest that

CPNE7 induces autophagy in both the pre-odontoblast and mature odontoblast states.

CPNE7 Promotes Odontoblast Differentiation and Dentin Formation by Inducing Autophagy in a Manner Different from That of Rapamycin

I next investigated how CPNE7 functions by inducing autophagy at each stage of odontoblast differentiation (pre-odontoblast and mature odontoblast). After treating both differentiation states with rCPNE7 for 24 h, I evaluated the expression levels of odontoblast differentiation and mineralization markers, DSP and DMP-1 proteins, respectively. Interestingly, rCPNE7 treatment significantly increased the expression levels of the odontoblast differentiation and dentin mineralization marker proteins in both states. To understand whether the CPNE7-induced autophagy regulated odontoblast differentiation and dentin mineralization, I used a PI3K inhibitor, 3-methlyadenine (3-MA), to block autophagic activity. When autophagic activity was inhibited in both differentiation states, the expression levels of LC3-II, DSP, and DMP-1 decreased. Interestingly, rCPNE7 treatment increased the expression levels of those proteins, but administering 3-MA after the rCPNE7 treatment counteracted the effects of rCPNE7 (Figure 2A). Therefore, CPNE7 promotes odontoblast differentiation and dentin mineralization by inducing autophagy. Next, I induced autophagy using rapamycin, a commonly used autophagy inducer, to compare its effects with those of CPNE7-induced autophagy in both differentiation states. Peculiarly, rapamycin-induced autophagy increased the levels of the odontoblast differentiation and mineralization marker proteins in

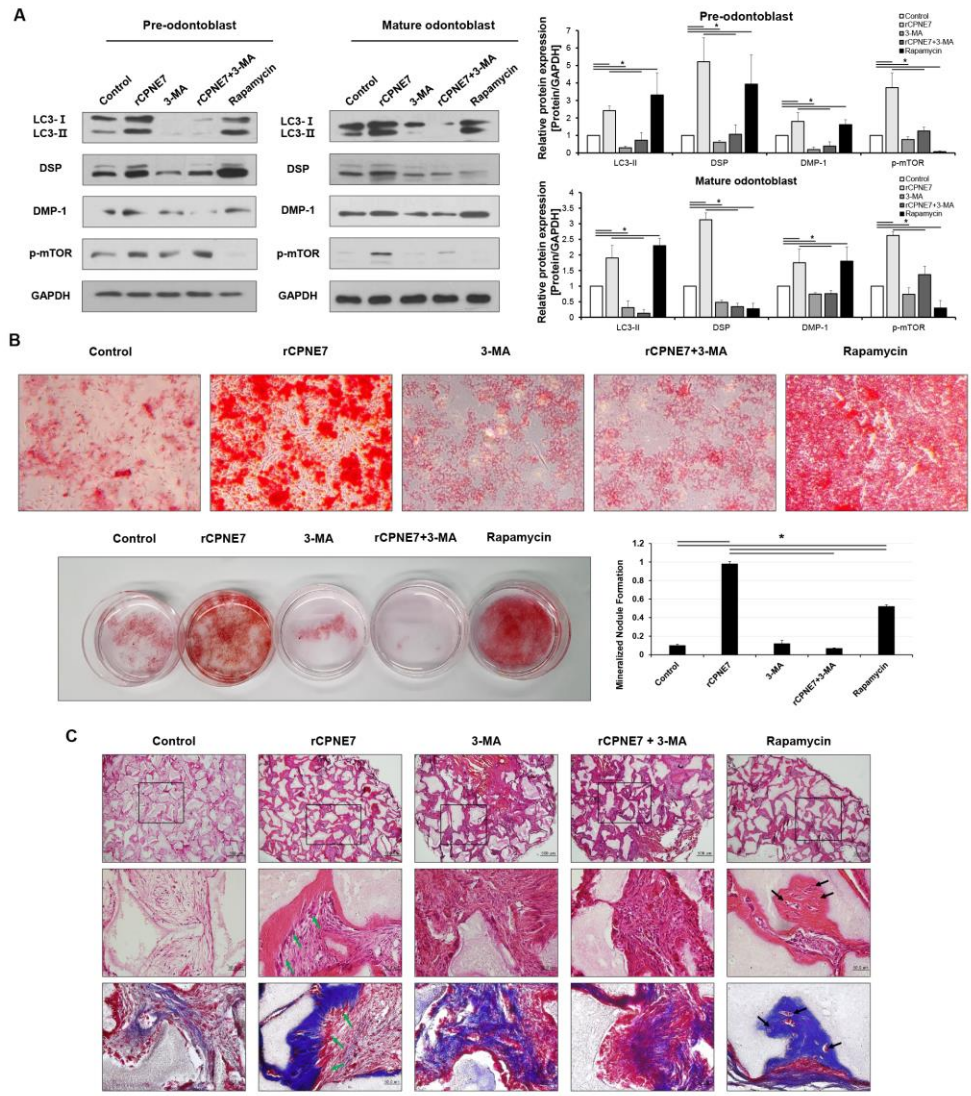

Figure 2. CPNE7 promotes odontoblast differentiation and dentin formation by inducing autophagy in mature odontoblasts. (A) Both stages of hDPCs were treated with rCPNE7 (100 ng/ml), 3-MA (5 mM), rCPNE7 + 3-MA, or rapamycin (10 nM) for 24 h. LC3 II, DSP, DMP-1, and p-mTOR protein levels were evaluated by western blot analysis. (B) Effects of rCPNE7, 3-MA, rCPNE7 + 3MA, and rapamycin on the mineralized nodule formation of mature hDPCs *in vitro*, as analyzed by alizarin red S staining. (C) Ectopic transplantation of mature

odontoblasts treated with control (PBS), rCPNE7, 3-MA, rCPNE7 + 3-MA, or rapamycin and HA/TCP was histologically analyzed through H&E and Masson's trichrome staining. Scale bars = 500 mm. Boxed areas are shown at higher magnification. Scale bars = 50 mm. Dentin-pulp-like structures (green arrows) were observed in the rCPNE7 groups. Cells entrapped in mineralized tissue (black arrows) were observed in the rapamycin groups. 3-MA, 3-methyladenine; DMP-1, dentin matrix protein 1; p-mTOR, phospho-mammalian target of rapamycin; HA/TCP, hydroxyapatite/tricalcium phosphate. Significant differences are shown with asterisks. *$P < 0.05$.

the pre-odontoblast state, similar to CPNE7-induced autophagy; however, in mature odontoblasts, rapamycin-induced autophagy increased the expression of DMP-1 but decreased the expression of DSP (Figure 2A). Thus, CPNE7- and rapamycin-induced autophagy are not identical in their function in mature odontoblasts.

To further elucidate the pathway between CPNE7- and rapamycin-induced autophagy, I evaluated the effects of CPNE7 and rapamycin on phosphorylated mTOR (p-mTOR), the inhibition of which induces autophagy. p-mTOR decreased after treatment with rapamycin, whereas it increased in the CPNE7-treated group (Figure 2A), suggesting that CPNE7 and rapamycin induce autophagy through different pathways in mature odontoblasts. Following that expression analysis, I analyzed the dentin formation capacity of mature odontoblasts *in vitro* and *ex vivo*. To analyze the capacity of dentin formation, most studies have focused on the entire process of odontoblast differentiation, from the stem cell stage to the mature odontoblast stage. However, those methods make it difficult to determine the capacity of dentin formation of mature odontoblasts. In this study, I analyzed the *in vitro* mineralization capacity of mature odontoblasts using cells at specific differentiation stages. Mature odontoblasts treated with rCPNE7 showed significantly more mineralized nodule formation than the control. The rapamycin-treated group also showed more mineralized nodules than the control, but its effects were weaker than those seen in the rCPNE7 group. On the other hand, the number of mineralized nodules was significantly reduced when 3-MA was administered alone or with rCPNE7 (Figure 2B and 3). Therefore, CPNE7 enhances the mineralization potential of mature odontoblasts by inducing autophagy.

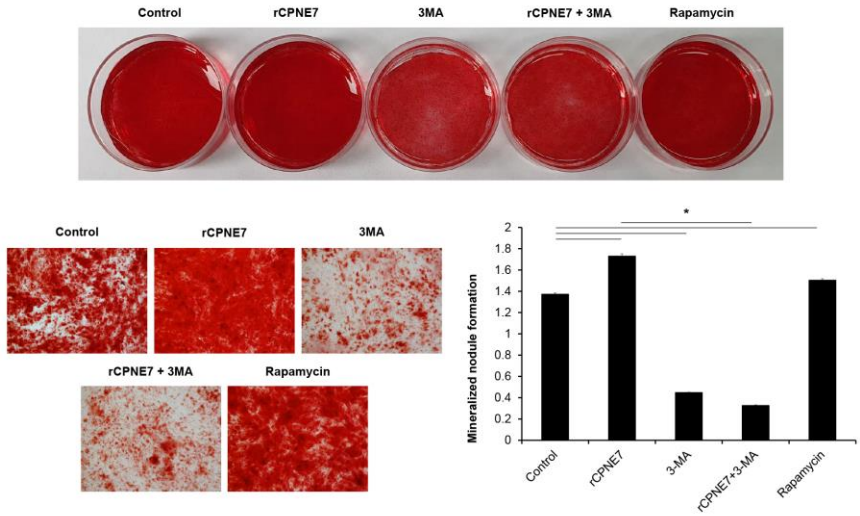

Figure 3. CPNE7 promotes mineralized nodule formation by inducing autophagy in mature odontoblast. Effects of rCPNE7, 3-MA, rCPNE7+3MA, and rapamycin on the mineralized nodule formation from day 14 to day 21, as analyzed by alizarin red S staining. Significant differences are shown with asterisks. **P* < 0.05.

I next tested the role of CPNE7-induced autophagy in enhancing the cellular activity and mineralization capacity of mature odontoblasts *ex vivo*. hDPCs differentiated until day 21 were transplanted into the subcutaneous tissues of immunocompromised mice along with hydroxyapatite/tricalcium phosphate (HA/TCP) in five different conditions: PBS treatment (control), rCPNE7-treatment (rCPNE7), 3-MA treatment (3-MA), rCPNE7 and 3-MA treatment (rCPNE7+3-MA), and rapamycin-treatment (rapamycin). After six weeks, the tissues newly formed around the HA/TCP were observed. Similar to our *in vitro* results, cellular function and physiological activity were debilitated in mature odontoblasts, and little hard tissue formation was observed in the control group (Figure 2B, C). The rCPNE7 group showed significantly more dentin-pulp-like tissue formation than the control, and the 3-MA group showed abnormal cell morphology and no hard tissue formation. The addition of 3-MA offset the effects of rCPNE7 because little hard tissue formation was observed in the rCPNE7+3-MA group. In the rapamycin group, a smaller amount of hard tissue was formed than in the rCPNE7 group, and irregular hard tissue in which cells were entrapped was observed. Masson's trichrome staining further confirmed that CPNE7 enhanced the mineralization capacity of mature odontoblasts and that autophagy inhibition impaired it *ex vivo* (Figure 2C). Thus, CPNE7 fosters the cellular activity and mineralization potential of mature odontoblasts in a way that depends on autophagy.

CPNE7 Stimulates Odontoblast Process Elongation

After demonstrating that CPNE7 induces tubular dentin formation (Figure 1A), I explored whether CPNE7 promotes odontoblast process elongation by examining changes in the expression levels of microtubule-associated proteins, TAU and NESTIN, in both differentiation states. TAU and NESTIN are terminally differentiated odontoblast marker proteins that participate in odontoblast morphogenesis by regulating microtubule organization and intermediate filaments, respectively (Miyazaki et al., 2015). rCPNE7 treatment remarkably increased the expression of both proteins compared to the control group. In contrast, the groups treated with 3-MA, alone or with rCPNE7, showed decreased expression levels in both differentiation states. Interestingly, the rapamycin group had significantly decreased TAU levels compared to the rCPNE7 group in both differentiation states, whereas the NESTIN levels decreased after rapamycin treatment in pre-odontoblasts and increased in mature odontoblasts, compared with the control (Figure 4A). Overall, the rapamycin group did not show obvious associations with cytoskeletal related markers, unlike the rCPNE7 group, which showed increases in both markers. Following that expression analysis, I conducted a cell morphological analysis to examine whether CPNE7 promotes physiological odontoblast process elongation in both differentiation stages. Under a light microscope, unidirectional odontoblast process-like structures were visible in the control groups of pre-odontoblasts and mature odontoblasts cultured in an odontoblast differentiation medium for 7 days. Morphologically, as odontoblasts differentiate, the cell bodies retreat by elongating their single cellular processes, known as the odontoblast process (Arana-Chavez and Massa, 2004). In both differentiation stages, the rCPNE7 group showed significantly longer unidirectional odontoblast process-like structures than the control group (Figure 5), and the rapamycin group showed

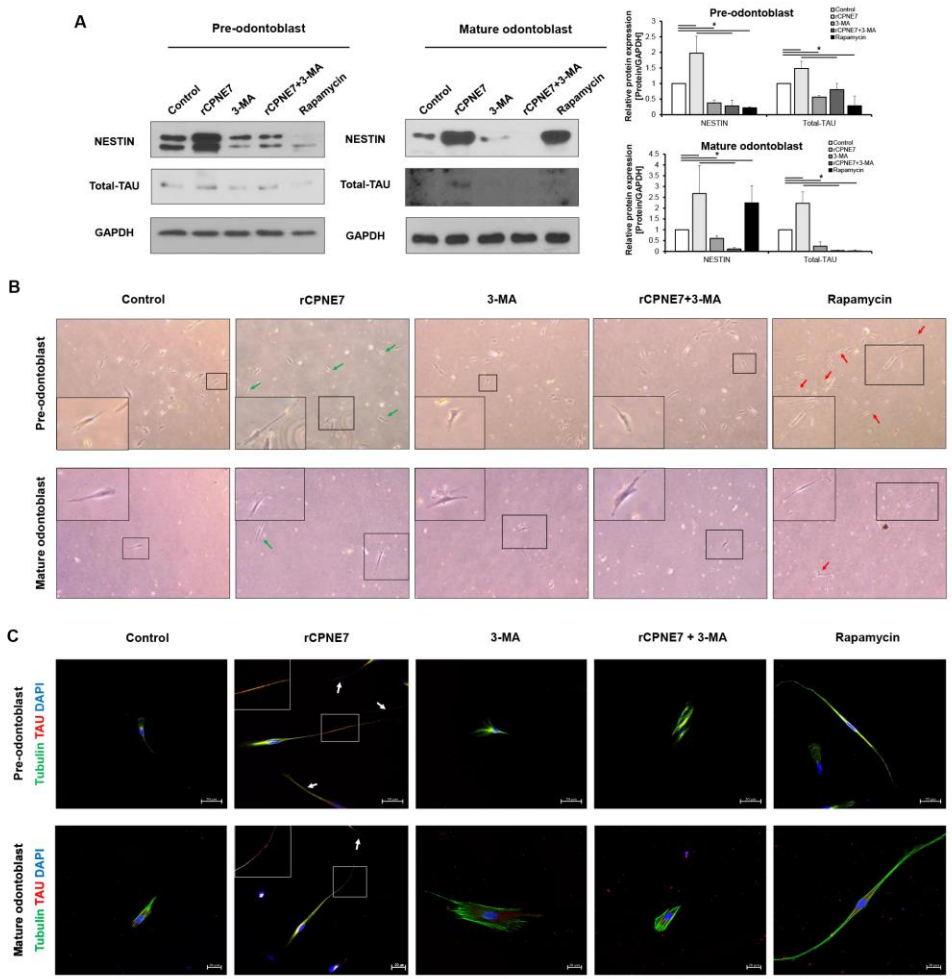

Figure 4. CPNE7 stimulates odontoblast process elongation. (A) Both stages of hDPCs were treated with rCPNE7, 3-MA, rCPNE7 + 3-MA, or rapamycin for 24 h. NESTIN and total-TAU protein levels were evaluated by western blot analysis. (B,C) The morphology of hDPCs was analyzed in each group 7 days after treatment. Boxed areas are shown at higher magnification. (B) Cells were observed under an optical microscope (100 x). Odontoblasts with a unidirectional odontoblast process-like structure (green arrows) were observed in the rCPNE7 group. Multidirectional odontoblast process-like structures were observed (red arrowheads) in the rapamycin group. (C) Representative immunofluorescence

images of TUBULIN (green) and TAU (red) in each group of treated cells. TUBULIN and TAU expression was co-localized in the odontoblast process-like structures in the rCPNE7 group (arrows). Scale bars = 50 mm and 20 mm. Significant differences are shown with asterisks. *$P < 0.05$.

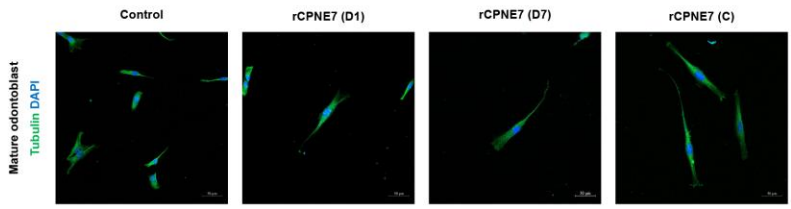

Figure 5. CPNE7 stimulates odontoblast process elongation in mature odontoblast. hDPCs were differentiated for 21 days with rCpne7 treatment for the following(indicated) period of time. At mature stage (D1; 20 – 21 days), secretory to mature stage (D7; 14 – 21 days), whole differentiation stage (C; continuously, 0 – 21 days) of odontoblast. Localization of TUBULIN (green) was observed by immunofluorescence. DAPI (blue) was counterstained to indicate the nucleus. Scale bars: 50 μm.

multidirectional cellular processes that differed from the typical physiological odontoblast morphology. Those cell morphologies were not observed in the autophagy-inhibited groups (Figure 4B). I further evaluated each of the cell morphologies by performing a co-immunofluorescence assay for TAU and TUBULIN. Similar to the western blotting, the rCPNE7 group showed elevated TAU expression in both stages of odontoblasts. Interestingly, in the rCPNE7 group, TAU was strongly co-localized with TUBULIN at the tip of the unidirectional odontoblast process-like structure, whereas co-localization was rarely seen in the other groups (Figure 4C). Thus, CPNE7 upregulates the expression of TAU and might be involved in cellular remodeling, and it eventually promotes odontoblast process elongation in both differentiation states.

CPNE7 Removes Lipofuscin from Mature Odontoblasts

Lipofuscin is a fluorescent pigment that accumulates with aging in the lysosomal compartment of post-mitotic cells such as odontoblasts and neurons (Rezzani et al., 2012). Because of the correlation between its accumulation and aging, lipofuscin has long been reported to be pathogenic (Terman and Brunk, 2004). Confocal microscope was used to check the accumulation of lipofuscin pigment following odontoblast differentiation *in vitro* (Figure 6A). I also identified the extent of lipofuscin accumulation in odontoblasts *in vivo* in post-natal day 2 mice (young mice) and post-natal 6-month-old mice (aged mice). Consistent with previous results, lipofuscin pigments were rarely observed in the early differentiating odontoblasts of young mice, and they amassed in the mature

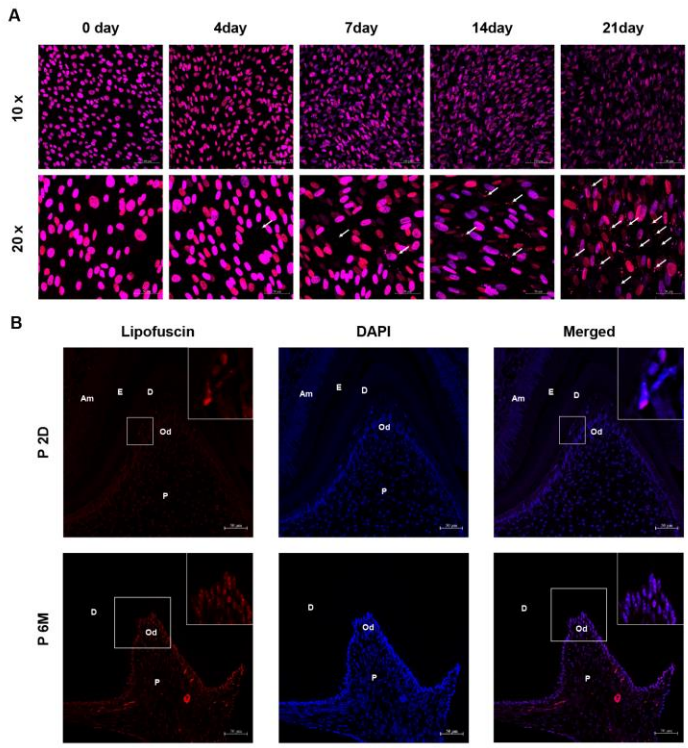

Figure 6. Lipofuscin progressively accumulated in mature odontoblasts. (A) Lipofuscin (red dots; white arrows) accumulation was observed during the differentiation of hDPCs. (B) Lipofuscin pigments were observed in mature odontoblasts on postnatal day 2 (P2D) and at postnatal 6 months (P6M). Scale bars = 50 mm. Boxed areas are shown at higher magnification. Scale bars = 10x: 100 mm and 20x: 50 mm. Am, ameloblast; E, enamel; P, pulp; Od, odontoblast; D, dentin.

odontoblasts of the aged mice (Figure 6B). Because I demonstrated that lipofuscin actually accumulates following differentiation and that the cellular function and physiological activity of mature odontoblasts are debilitated, our next question was whether CPNE7-induced autophagy could eliminate lipofuscin. Interestingly, treating mature odontoblasts with rCPNE7 decreased the accumulation of lipofuscin compared with the control and autophagy-inhibited groups. In the rapamycin-treated group, however, lipofuscins were observed to a greater extent than in the rCPNE7-treated group in mature odontoblasts (Figure 7). These results suggest that CPNE7-induced autophagy could cause long-lived post-mitotic odontoblasts to revert to the cellular function and physiological activity of their active state, perhaps by removing lipofuscin.

CPNE7 Promotes Physiological Dentin Formation *in vivo*

A mouse molar defect model with exposed dentinal tubules was created using drilling to evaluate the role of CPNE7-induced autophagy in mature odontoblasts and physiological dentin formation *in vivo*. The defects were topically treated with PBS (control), rCPNE7, 3-MA, rCPNE7+3-MA, or rapamycin. The exposed dentin areas of the five groups were filled with GI cement after the topical treatment, and the reactions of the mature odontoblasts were histologically analyzed 4 weeks later. In the control group, no changes were observed. However, in the rCPNE7 group, a large amount of tubular dentin formation was observed below the dentinal defect site. In the 3-MA group, I observed a hard tissue without dentinal tubule structure entrapping a small number of cells. Interestingly, in the

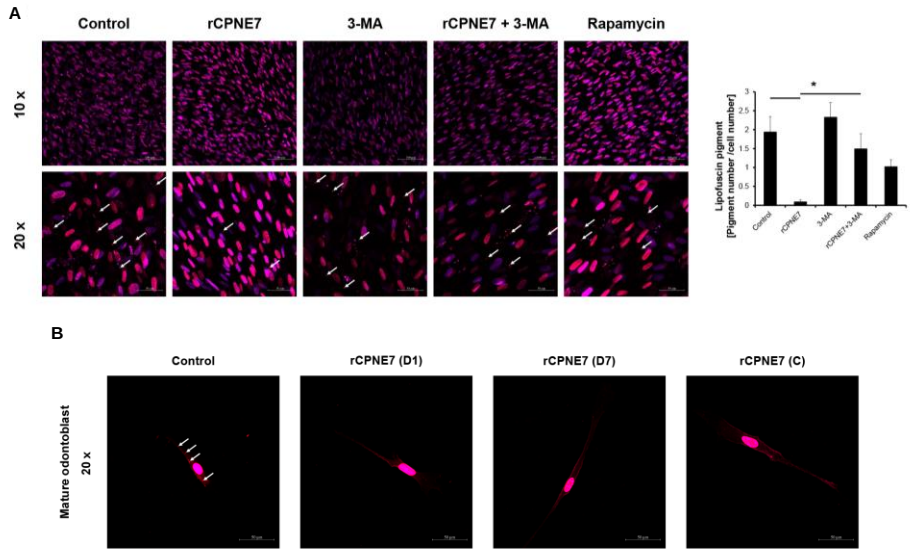

Figure 7. CPNE7 removed lipofuscin in mature odontoblasts. (A) Lipofuscin was analyzed in the control, rCPNE7, rCPNE7 + 3-MA, and rapamycin groups of mature odontoblasts. (B) hDPCs were differentiated for 21 days with rCpne7 treatment for the following(indicated) period of time. At mature stage (D1; 20 – 21 days), secretory to mature stage (D7; 14 – 21 days), whole differentiation stage (C; continuously, 0 – 21 days) of odontoblast. Lipofuscin (red dots; white arrows) was observed by immunofluorescence. DAPI (blue) was counterstained to indicate the nucleus. Scale bars: 50 μm. Significant differences are shown with asterisks. *P < 0.05.

group that treated CPNE7 and 3-MA together, dentin was formed, but the odontoblast process was hardly seen. Similar to our *in vitro* cell morphological analysis, the rapamycin-treated odontoblasts formed dentin with irregular and entangled cellular processes *in vivo* (Figure 8A, B). Furthermore, compared to the control group, LC3-positive odontoblasts and clearly removed lipofuscin were detected below the newly formed tubular dentin in the rCPNE7 group. However, no LC3-postive odontoblasts and large amounts of lipofuscins were observed in autophagy-inhibited groups. Although some LC3 positive cells were detected, the lipofuscin pigments were still observed in Rapamycin-treated group *in vivo*, similar to the results of *in vitro* experiments. (Figure 8C, D). Thus, CPNE7-induced autophagy might reactivate the debilitated physiological activity of mature odontoblasts and promote the formation of physiological dentin.

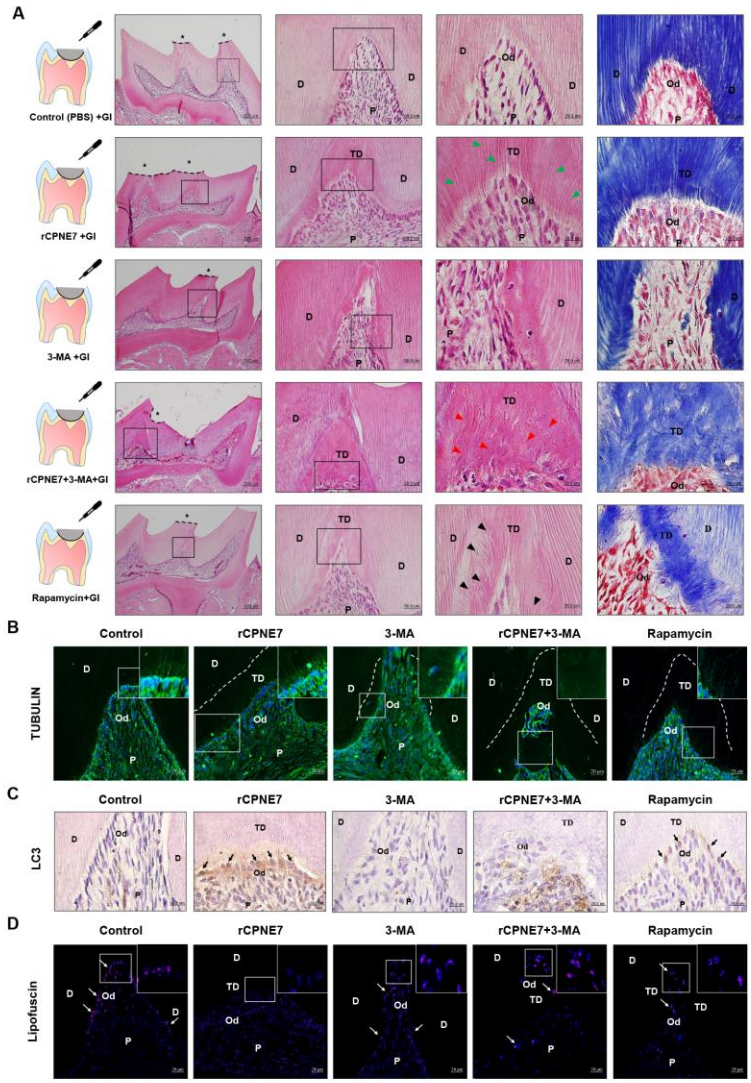

Figure 8. CPNE7 promotes the formation of dentin *in vivo*. (A) Schematic diagrams of the mouse molar defect model. The defect areas were covered with glass ionomer (GI) cement after topical treatment: control (PBS + GI), rCPNE7 (rCPNE7 + GI), 3-MA (3-MA + GI), rCPNE7 and 3-MA (rCPNE7 + 3-MA + GI), or rapamycin (rapamycin + GI). Histologic analysis of the defect areas were performed 4 weeks later using H&E and Masson's trichrome staining. Scale bars = 200 mm. Boxed areas are shown at higher magnification. Scale bars = 50 mm and

20 mm. Odontoblast process-like structures (green arrowheads) were observed in the rCPNE7 + GI group. Few odontoblast process-like structures (red arrowheads) were observed in the rCPNE7 + 3-MA + GI group. Irregular and entangled cellular processes (arrowheads) were observed in the rapamycin + GI group. (B) Representative immunofluorescence images of tubulin (green). Dotted line shows the boundary of tubular dentin newly formed from native dentin. (C) LC3 expression (black arrow) was detected by immunohistochemistry. (D) Lipofuscin pigments (white arrows) were observed in odontoblasts at 488 nm. Scale bars = 20 mm. Boxed areas are shown at higher magnification. P, pulp; Od, odontoblast; D, dentin; TD, tubular dentin.

IV. DISCUSSION

Autophagy is a highly conserved, lysosome-mediated, self-degradation mechanism that allows cells and tissues to cope with stimuli such as starvation, infection, and pharmacological agents. In physiological conditions, this cellular system finely regulates processes indispensable for development, differentiation, and survival (Rabinowitz and White, 2010). The inhibition of autophagy in mouse tooth germs contributes to the loss of odontoblast polarization and poor differentiation, which eventually lead to highly disrupted tooth morphology (Park et al., 2020). Thus, the proper modulation of autophagic activity is essential for odontoblast differentiation and physiological dentin formation. Moreover, mature odontoblasts, whose secretory machinery and autophagic activity are reduced, do not react properly to external stimuli (Couve, 1986). In this study, the cellular activity and dentin formation capability of mature odontoblasts became debilitated as autophagic activity decreased. If autophagic activity could be increased in mature odontoblasts, their cellular activity and dentin formation ability might revert to that of active secretory odontoblasts.

In this study, I found that CPNE7-induced autophagy increased the expression of odontoblast differentiation and mineralization marker proteins in both pre-odontoblasts and mature odontoblasts. The effects of rapamycin treatment on pre-odontoblasts and mature odontoblasts differed from those of CPNE7-induced autophagy. Rapamycin-induced autophagy promoted odontoblast differentiation by upregulating DSP and DMP-1 in pre-odontoblasts, similar to CPNE7-induced autophagy. However, in mature odontoblasts, the DSP expression level in the rapamycin group decreased, unlike the results from CPNE7-induced

autophagy. There are two types of autophagy-induced pathway: mTOR-dependent and independent. As a general autophagy inducer and p-mTOR inhibitor, Rapamycin was used in our experiment. Indeed, the expression of p-mTOR and LC3-II was decreased and increased respectively in rapamycin-treated both differentiation stages of odontoblasts. This result suggests that Rapamycin-induced autophagy is an mTOR-dependent autophagy pathway. However, when CPNE7 was treated in both stages of odontoblasts, p-mTOR and LC3-II were increased, which suggests CPNE7 could induce autophagy through mTOR-independent pathway, and this CPNE7-induced autophagy may have different functions than the mTOR-dependent autophagy pathway. Furthermore, mTOR is the master regulator of cell growth, promoting anabolic processes like protein translation. The activity of mTOR is also regulated by changes in energy states (Al-Bari and Xu, 2020). For the cells in need of massive protein secretion, the simultaneous coupling of autophagy and mTOR is occurring to handle rapid protein turnover. (Narita et al., 2011). When CPNE7-induced autophagy in an mTOR-independent manner change the energy states of mature odontoblast, it simultaneously could promote protein expression for dentin mineralization and odontoblast process formation by activating the mTOR pathway.

Odontoblast processes and dentinal tubules are typical morphological characteristics of the physiological dentin-pulp complex. During dentin formation, the odontoblast process is elongated gradually as a direct extension of the cell body, along with continuous remodeling of the plasma membrane. The odontoblast process sequentially secretes matrix vesicles and is eventually surrounded by a calcified matrix, the dentinal tubule. The odontoblast process consists mostly of a

cytoskeleton, including microtubules. It has been suggested that the microtubules not only serve a cytoskeletal function but also play a role in the transport of release of matrix vesicles (Lee et al., 2014b). In any case, odontoblast process formation and elongation are essential for physiological dentin formation. In this study, I observed that long unidirectional odontoblast processes were formed in response to CPNE7-mediated autophagy in both stages of odontoblasts. On the other hand, rapamycin treatment of both stages of odontoblasts produced multidirectional cellular processes. Furthermore, increased expression levels of TAU were observed after CPNE7 treatment, while they decreased after rapamycin treatment. TAU is a neuronal phosphoprotein that modulates microtubule dynamics and assembly and has various neuronal developmental functions. Moreover, TAU and TUBULIN are co-expressed in odontoblasts upon the onset of dentinogenesis, and they are localized mainly in the apical regions of the cell body and cell processes, similarly to the expression patterns seen for NESTIN in mature odontoblasts (Miyazaki et al., 2015). Our confocal microscopy results confirm that TAU expression increased and was co-localized with TUBLIN in rCPNE7-treated unidirectional odontoblast processes. The co-localization of TAU and TUBLIN was not observed in the rapamycin-treated multidirectional cellular processes. In the case of neurons, autophagy regulates neurite outgrowth and exon growth by stabilizing microtubules (Crawley and Grill, 2021). Moreover, the mTOR pathway also modulates neuronal polarity by inducing the local translation of TAU protein (Morita and Sobue, 2009). Although Rapamycin can also elongate odontoblast process-like structure through autophagy induction in mature odontoblasts, its morphology is different due to a lack of mTOR-TAU pathway. Thus, only CPNE7-induced autophagy can promote the formation and elongation of physiological

odontoblast processes. The reason behind the multidirectional cellular process after the rapamycin treatment requires further research.

Mature or terminally differentiated cells that no longer undergo mitosis, including odontoblasts, neurons, and cardiomyocytes, are called long-lived post-mitotic cells (Terman et al., 2010). Long-lived post-mitotic cells, including odontoblasts, amass lipofuscin, which is regarded as a reliable biomarker of aging cells. The main cause of lipofuscin formation is the incomplete lysosomal degradation of damaged mitochondria. Autophagic activity fails to function properly as lipofuscin accumulates in mature odontoblasts, which eventually compromises cellular activity (Couve et al., 2013). Since the case of lipofuscin degradation or exocytosis are rarely reported, the removal of lipofuscin is regarded as impossible so-called indigestible. Therefore, retarding its accumulation is the best way to treat lipofuscin. Long-lived post-mitotic cells are particularly vulnerable to lipofuscin due to its limitation of diluting lipofuscin by mitosis (Brunk and Terman, 2002). Recent studies showed the possibility of removing lipofuscin through autophagy induction (Martinez-Cisuelo et al., 2016; Chen et al., 2018; Li et al., 2021). In this study, in the autophagy-inhibited groups (3-MA and rCPNE7+3-MA), a large amount of lipofuscin was observed in mature odontoblasts similarly to that of the control group. Interestingly, when CPNE7 was administered to mature odontoblasts *in vitro* and *in vivo*, most of the lipofuscin was removed, whereas rapamycin treatment did not clearly eliminate lipofuscin. Thus, CPNE7-induced autophagy could cause mature odontoblasts to revert to the cellular function and physiological activity of active secretory odontoblasts by removing lipofuscin. The precise mechanism by which CPNE7-induced autophagy

eliminates lipofuscin from mature odontoblasts requires further study.

In this study, rCPNE7 treatment of exposed dentin generated a massive area of tubular dentin containing physiological odontoblast processes, whereas rapamycin treatment produced a narrow area of dentin containing irregular and entangled odontoblast processes. Furthermore, the mature odontoblasts in the rCPNE7-treated group contained less lipofuscin under the newly formed dentin than the control group. The most interesting finding was that when CPNE7 and 3-MA were administered to the defective dentin together, dentin formation was disrupted and showed few odontoblast processes. Therefore, CPNE7-induced autophagy is an innovative process for reactivating the cellular activity of and removing lipofuscin from mature odontoblasts. That process promotes odontoblast process elongation and dentin formation, which eventually leads to physiological dentin regeneration (Figure 9).

In conclusion, the findings of the present study hint the potential application of CPNE7-mediated autophagy in mature odontoblast's cellular activity reactivation and physiological dentin regeneration in treating dentinal defects. More specifically, CPNE7 was seen to promote physiological odontoblast process elongation and dentin formation. In addition, while exploring CPNE7-induced autophagy, I observed lipofuscin elimination and TAU protein modulation at cell projection, which mirror the possibility of CPNE7 reactivating long-lived post mitotic cells, such as neuron cells. On the top of its CPNE7's potential application in dentin regeneration and dental pulp protection, this possibility suggests that CPNE7-induced autophagy may be a potential therapeutic material for neurodegenerative diseases. Therefore, further studies are needed to elucidate the effects of CPNE7-

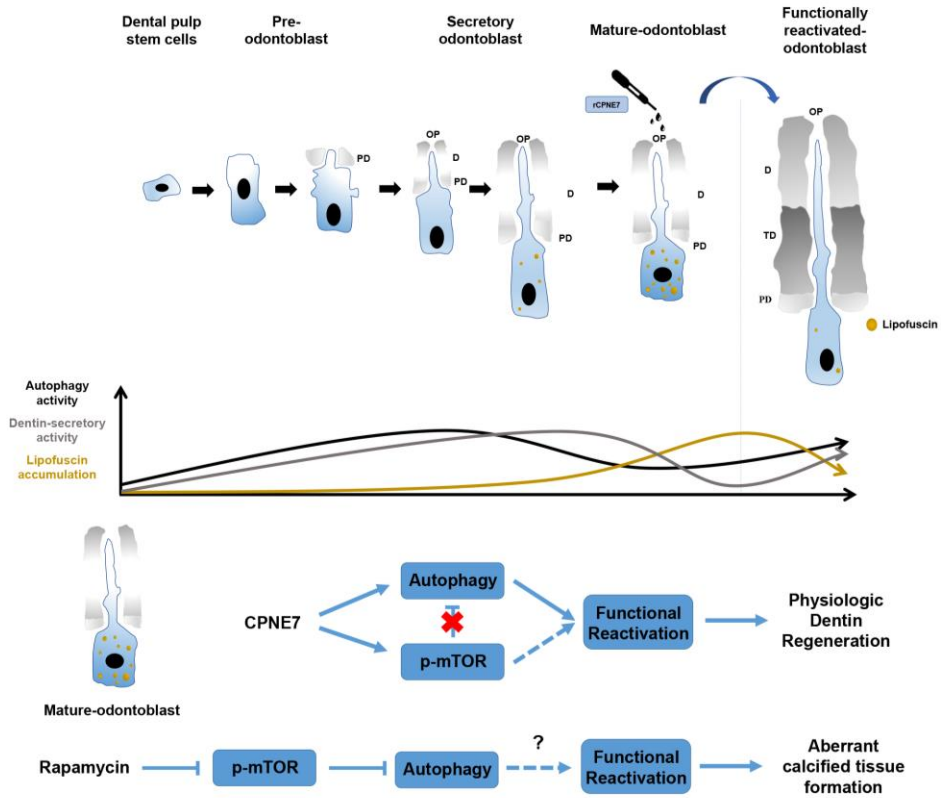

Figure 9. Schematic illustration of the effects of CPNE7 in mature odontoblasts. Dental pulp stem cells have the potential to differentiate into pre-odontoblasts, secretory odontoblasts, and mature odontoblasts. Physiologically, the cellular activities of odontoblasts, such as dentin secretion and process elongation, increase gradually during the early differentiation stage, similar to the increasing autophagy activity. Both the cellular activities of odontoblasts and autophagic activity decrease steadily in mature odontoblasts. Moreover, lipofuscin, an aging pigment, progressively accumulates in mature odontoblasts. Rapamycin-induced autophagy could not properly restore the physiological activity of mature odontoblasts. However, CPNE7-induced autophagy functionally reactivated mature odontoblasts and produced physiological dentin formation.

induced autophagy and whether it induces functional reactivation in other long-lived post mitotic cells.

CHAPTER III.

Different Responsiveness of Alveolar Bone and Long Bone to Epithelial-Mesenchymal Interaction-Related Factor

*** This chapter has been largely reproduced from an article published by Son C and Park JC. (2020). JBMR Plus., 4(8): e10382.**

I. ABSTRACT

Alveolar bone is both morphologically and functionally different from other bones of axial or peripheral skeleton. Due to its sensitive nature to external stimuli including mechanical stress, bone loss stimuli, and medication-related osteonecrosis of the jaw (MRONJ), alveolar bone rendering is seen as an important factor in various dental surgical processes. While multiple studies have validated the response of long bone to various factors, how alveolar bone responds to functional stimuli still needs further clarification.

In this study, to examine the characteristics of bone *in vitro*, I isolated cells from alveolar, femur, and tibia bone tissue. Although primary cultured mouse alveolar bone-derived cells (mABDC) and long bone-derived cells (mLBDC) exhibited similar osteoblastic characteristics, morphology, and proliferation rates, both showed distinct expression of neural crest (NC) and epithelial-mesenchymal interaction (EMI)-related genes. Furthermore, they showed significantly different mineralization rates. RNA sequencing data demonstrated distinct transcriptome profiles of alveolar bone and long bone. Osteogenic, NC and EMI-related genes showed distinct expression between mABDC and mLBDC. When the gene expression patterns during osteogenic differentiation were analyzed, excluding several osteogenic genes, NC, and EMI-related genes showed different expression patterns. Among EMI-related proteins, BMP4 elevated the expression levels of osteogenic genes, Msx2, Dlx5, and Bmp2 the most, more noticeably in mABDC than mLBDC during osteogenic differentiation. *In vivo* models, BMP4-treated mABDC group showed massive bone formation and maturation than its counterpart. BSP expression was also validated in calcified tissues.

Overall, our data suggests that alveolar bone and long bone have different responsiveness to EMI by distinct gene regulation. In particular, BMP4 has critical bone formation effects on alveolar bone than on long bone.

II. INTRODUCTION

Tooth takes many mechanical stress from a variety of external forces involving mastication, tooth brushing, and injury (Naveh et al., 2012). Against this stress, periodontium – tissue covering tooth root – supports the tooth (Cho and Garant, 2000). Among the tissues that consist periodontium, alveolar bone have interesting conformation changes sensitive to external forces. At times, such bone sensitivity allows rearrangement of the tooth to its proper site (D.McKee, 2000). As hinted, the condition of alveolar bone is clinically significant in many cases including periodontitis and dental implant surgery (Papapanou et al., 2018; Greenwell et al., 2019). However, the development and underlying genetic characteristics of alveolar bone still requires further investigation.

To understand the genetic and molecular makeup of alveolar bone, I selected long bone as the comparison due to its preexisting extensive research. When compared, alveolar and long bone showed different responsiveness. Generally, bone is a dynamic tissue that responds to environmental stimuli. For example, reduction of mechanical loading on bone results in bone loss (Metzger et al., 2017). Although bone does generally respond to environmental stimuli, alveolar bone is especially sensitive to mechanical forces (D.McKee, 2000). Such sensitivity has been taken advantage of for orthodontic tooth movement. Another difference in responsiveness can be seen in osteoporosis treatment. When treated with osteoporosis drugs, long bone has shown positive results. In contrast, alveolar bone has shown detrimental effects from the same drugs; however, the probability of the effect arising is low (Rosella et al., 2016; Nicolatou-Galitis et al., 2019). These different phenomena infer that fundamental differences exist between

alveolar bone and long bones.

Previous studies have suggested that the developmental process of alveolar and long bone is different. Especially, epithelial-mesenchymal interaction (EMI) is known to play an essential role in organ development – including bone (Ribatti and Santoiemma, 2014). Early development of both alveolar bone and long bone is closely related to EMI. For long bone, the formation of limb bud emerges from the interaction between apical ectodermal ridge, a specialized epithelium, and mesenchyme, which is derived from lateral plate mesoderm (Zeller et al., 2009). For alveolar bone, the development of periodontium results from the interaction between dental epithelium and ectomesenchyme – a form of mesenchyme that migrates from neural crest (NC) (Lumsden, 1988). Moreover, recent studies give evidence about the linkage between alveolar bone remodeling and epithelial cell rests of Malassez in adult periodontium (Silva et al., 2017). Using these differences in EMI interaction this paper attempts to understand the uniqueness in alveolar bone using developmental differences.

In this study, I found distinct genetic profiles of EMI-related genes, NC-related genes, and osteogenic genes by investing transcriptome data in mouse primary cultured alveolar bone-derived cells (mABDC) and long bone-derived cells (mLBDC). The EMI-related factors produced by dental epithelium showed different effects in mABDC and mLBDC. Finally, our results provided evidence that BMP4 regulates bone formation differently in alveolar bone and long bone.

III. MATERIALS AND METHODS

Tissue preparation and histology

All animal experiments followed protocols approved by the Institutional Animal Care and Use Committee of Seoul National University (SNU-160509-6). The head and long bone dissected from C57BL/6 male mice were fixed in 4% paraformaldehyde (PFA; Sigma-Aldrich, St. Louis, MO, USA) at 4 °C overnight and decalcified in a 10% ethylenediaminetetraacetic acid solution (EDTA; Georgiachem, Suwanee, GA, USA) for 2 weeks at room temperature. Embedded tissues were sectioned at a thickness of 5 μm. To evaluate histologic findings, sections were stained with hematoxylin and eosin (H&E) (Vector Labs, Burlingame, CA, USA). For histomorphometric analysis, an optical microscope (BX50, Olympus Co., Tokyo, Japan) connected to a computer and charge-coupled device (CCD) camera (DP71, Olympus Co.) and an adaptor (U-TV0.63XC, Olympus Co.) was used to take images of the samples. Image analysis of new bone and marrow formation was performed with analySIS LS Starter (Olympus Soft Imaging Solutions GmbH, Muenster, Germany).

Primary cell culture

Alveolar and long bones were collected from seven-day-old C57BL/6 mice. After euthanasia, the alveolar, tibia and femur bones were removed and cells were released from the matrix using 1 ml digestion medium [0.1% Collagenase type I (GIBCO, Waltham, MA, USA), 0.2% dispase (GIBCO) diluted in α-MEM

(GIBCO)] at 37 °C with shaking. After 5 min digestion, first fraction was collected and discarded, and four subsequent fractions were collected in every 10 min and pooled. Cells were plated in α-MEM containing 10% fetal bovine serum (FBS; GIBCO) and antibiotic-antimycotic reagents (GIBCO) (proliferation medium) in 10 cm dishes. Cells were allowed to proliferate until 80–90% confluency and seeding into 6 cm dishes cultured until confluency (day 0 time point). Osteogenic differentiation was induced with 5 mM sodium beta-glycerophosphate (Sigma-Aldrich) and 50 µg/µl ascorbic acid (Amresco, Solon, OH, USA) in proliferation medium. Differentiation medium was changed every 2–3 days. Samples were collected at 0, 4, 7, 10 and 14 days by thoroughly rinsing the wells with PBS, and stored in −80 °C

Real-time PCR analysis

Total RNA was extracted from cells with Tri reagent according to the manufacturer's instructions (MRC, Cincinnati, OH, USA). Total RNA (3 µg) was reverse transcribed using Superscript IV reverse transcriptase (Invitrogen, Carlsbad, CA, USA) and oligo (dT) primers (Invitrogen). One µl of the RT product was PCR amplified using the primer pairs. For real-time PCR, the specific primers for *Bsp, Osteocalcin* (Oc), *Alp, Runx2, Osx, Bmp2, Bmp4, Nfic, Cpne7, Msx1, Msx2, Dlx5* and *Dmp1* were synthesized as listed in Table 1. Real-time PCR was performed on a Step One Plus sequence detection system (Applied Biosystems, Foster City, CA, USA) using iTaq™ Universal SYBR® Green Supermix (Bio-Rad Laboratories, Hercules, CA, USA) according to the manufacturer's instructions. PCR conditions

Table 1. Primers used for real-time PCR.

Genes	Primers
mGapdh	F 5'-AGGTCGGTGTGAACGGATTTG-3' R 5'-TGTAGACCATGTAGTTGAGGTCA-3'
mBsp	F 5'-CCGGCCACGCTACTTTCTT-3' R 5'-TGGACTGGAAACCGTTTCAGA-3'
mOC	F 5'-CTGACAAAGCCTTCATGTCCAA-3' R 5'-GCGCCGGAGTCTGTTCACTA-3'
mAlp	F 5'-CCAACTCTTTTGTGCCAGAGA-3' R 5'-GGCTACATTGGTGTTGAGCTTTT-3'
mRunx2	F 5'-TTCTCCAACCCACGAATGCAC-3' R 5'-CAGGTACGTGTGGTAGTGAGT-3'
mOsx	F 5'-CCCACCCTTCCCTCACTCAT-3' R 5'-CCTTGTACCACGAGCCATAGG-3'
mDmp1	F 5'-CATTCTCCTTGTGTTCCTTTGGG-3' R 5'-TGTGGTCACTATTTGCCTGTC-3'
mMsx1	F 5'-GAAACTAGATCGGACCCCGTGGAT-3' R 5'-GCTTGCGGTTGGTCTTGTGCTT-3'
mMsx2	F 5'-TTCACCACATCCCAGCTTCTA-3' R 5'-TTGCAGTCTTTTCGCCTTAGC-3'
mDlx5	F 5'-CTGGCCGCTTTACAGAGAAG-3' R 5'-TCACCTGTGTTTGCGTCAGT-3'
mBmp2	F 5'-GGGACCCGCTGTCTTCTAGT-3' R 5'-TCAACTCAAATTCGCTGAGGAC-3'
mBmp4	F 5'-TTCCTGGTAACCGAATGCTGA-3' R 5'-CCTGAATCTCGGCGACTTTTT-3'
mNfic	F 5'-GACCTGTACCTGGCCTACTTTG-3' R 5'-CACACCTGACGTGACAAAGCTC-3'
mCpne7	F 5'-CGGGACCCATTGACCAAGTC-3' R 5'-CATACACCTCAAACCGTAGCTTC-3'

were 40 cycles at 95 °C for 15 s, and 60 °C for 1 min. All reactions were performed in triplicate, and PCR product levels were normalized to that of the housekeeping gene, glyceraldehyde 3-phosphate dehydrogenase (Gapdh). Relative changes in gene expression were calculated using the comparative threshold cycle (C_T) method.

Alizarin red S staining for mineralized matrix

Cells were seeded into 6 cm culture dishes at a density of 0.8×10^5 cells per dish. Osteogenic differentiation was induced since dish reached confluency. At certain time point, cells were fixed with 4% PFA for overnight at 4 °C, and stained with 40 mM Alizarin red S (ARS; Sigma-Aldrich), pH 4.2 for 30 min at room temperature. For the quantification of mineralized matrix in culture, Alizarin red S stain was eluted using 0.5 ml of 5% sodium dodecyl sulfate (SDS; Amresco) in 0.5N HCl solution with shaking for 30 min and the absorbance of the eluted dye was measured at 405 nm.

Cell proliferation assay

Cells were seeded in a 96-well plate at 5000 per well in a CO2 incubator at 37°C in triplicates, and the samples were processed for MTT assay at day 0, 1, 2, and 3. One hundred fifty microliters of 5 g/l 3-(4,5-dimethyl-2-thiazolyl)-2,5-diphenyl-tetrazolium bromide (MTT) solution were added to each well for 2 hours at 37°C. The cells were then lysed in DMSO (Duksan, Korea), and absorbance at

570 nm was determined with a microplate reader.

mRNA-seq data

In order to construct cDNA libraries with the TruSeq RNA library kit, 1ug of total RNA was used. The protocol consisted of polyA-selected RNA extraction, RNA fragmentation, random hexamer primed reverse transcription and 100nt paired-end sequencing by Illumina HiSeq2500. The libraries were quantified using qPCR according to the qPCR Quantification Protocol Guide and qualified using an Agilent Technologies 2100 Bioanalyzer.

I processed reads from the sequencer and aligned them to the *Mus musculus (mm10)* using Tophat v2.0.13 (Trapnell et al., 2009). Tophat incorporates the Bowtie v2.2.3 (Langmead et al., 2009) algorithm to perform the alignment and mapping. Transcript assembly and abundance estimation using Cufflinks (Trapnell et al., 2010). After aligning reads to genome Cufflinks v2.2.1 were used to assemble aligned reads into transcripts, and to estimate their abundance. The transcript counts in isoform level were calculated, and the relative transcript abundances were measured in FPKM (Fragments per kilobase of exon per million fragments mapped) from Cufflinks. And gene level expression values were also calculated from the transcript counts. I excluded genes with zeroed FPKM values more than one for total samples. I added 1 with FPKM value of the filtered gene to facilitate log2 transformation. Filtered data was transformed by logarithm and normalized by the quantile normalization method.

I used multidimensional scaling (MDS) method to visualize the

similarities among samples. Hierarchical clustering analysis also was performed using complete linkage and Euclidean distance as a measure of similarity to display the expression patterns of DEGs which are satisfied with |fold change|≥2. Biologically gene functional annotation analysis for DEG list was performed using DAVID tool (http://david.abcc.ncifcrf.gov/) to understand biological meanings behind large list of genes (Huang da et al., 2009).

All data analysis and visualization of differentially expressed genes was conducted using R.

Western blot analysis

The whole cell lysates of cells were harvested using a lysis buffer consisting of 50 mM Tris–HCl, pH 7.4, 150 mM NaCl, 1% Nonidet P-40, 1 mM EDTA, and 1 mM PMSF supplemented with protease inhibitors (Roche Molecular Biochemicals, Mannheim, Germany). Following centrifugation at 13,000 x g for 30 min, the supernatant was collected for analysis. Protein concentrations were determined using the DC^{TM} protein assay system (Bio-Rad). Proteins (20 μg) were resolved using 10% polyacrylamide gel electrophoresis and transferred to a PVDF membrane (Merck Milipore, Billerica, MA, USA). The PVDF membrane was blocked with TBST (20 mM Tris-buffered saline, pH 7.4 (Tech&Innovation, Gangwon, Korea), and 0.1% Tween-20 (Amresco)) buffer containing 5% non-fat dry milk (Becton Dickinson, BD; Franklin Lakes, NJ, USA) for 1 h at room temperature. The blots were then washed and incubated with the indicated antibodies for overnight at 4 °C with gentle shaking. Affinity-purified rabbit

polyclonal anti-CPNE7, anti-NFIC and anti-BSP antibodies were produced as described previously (Lee et al., 2011a; Lee et al., 2011b). The anti-ALP (sc-30203), anti-RUNX2 (sc-10758) and anti-GAPDH (sc-25778) antibodies were purchased from Santa Cruz Biotechnology (Santa Cruz, CA, USA). The anti-OC (ab223692), anti-BMP2 (ab14933), anti-BMP4 (ab39973), anti-MSX1 (ab174207), anti-MSX2 (ab223692) and anti-DLX5 (ab64827) antibodies were purchased from Abcam (Cambridge, MA, USA). The anti-OSX (PA5-40509) was purchased from Invitrogen. Blots were washed three times for 10 min each in TBST, followed by incubation with anti-rabbit or anti-mouse immunoglobulin G conjugated to horseradish peroxidase (Santa Cruz Biotechnology) in TBST for 1 h at room temperature. After washing three times in TBST, the blots were analysed using an enhanced chemi-luminescence reagent (ECL; Dogen, Cambridge, MA, USA) according to the manufacturer's guidelines. Protein loading was assessed by the expression of GAPDH.

Ectopic transplantation *in vivo*, and histological analysis

The primary cultured mouse bone-derived cells (1 x 10^6) were mixed with 100 mg hydroxyapatite/tricalcium phosphate (HA/TCP) ceramic powder (Zimmer, Warsaw, IN, USA) alone, or with BMP4 (5 μg; Peprotch, Rocky Hill, NJ, USA) in an 0.5% fibrin gel, and then transplanted subcutaneously into immunocompromised mice (NIH-bg- nu-xid; Harlan Laboratories, Indianapolis, IN, USA) for 6 and 12 weeks.

For histomorphometric analysis of newly formed mineralized tissue,

Samples were harvested and fixed in 4% PFA, decalcified in 10% EDTA (pH 7.4), embedded in paraffin, and stained with H&E, Masson's trichrome (Polysciences Inc., Warrington, PA, USA), or processed for immunohistochemistry. For immunohistochemistry, proteins were detected with anti-BSP (Lee et al., 2011b) at a dilution of 1:100 as the primary antibody and a biotin-labeled goat anti-rabbit IgG (Vector Labs) as the secondary antibody. Tartrate resistant acid phosphatase (TRAP) staining was performed. The total mineralized area among the regenerated bone- and marrow-like tissue was analyzed using the LS starter program (Olympus Soft Imaging Solutions, Münster, Germany).

Statistical analysis

All values are expressed as mean ± SD (standard deviation) of at least three independent experiments. The student's *t*-test was used for comparison between two groups. The 2-way ANOVA was used for comparison more than three groups. Differences were considered statistically significant at $*p < 0.05$, and $**p < 0.005$.

IV. RESULTS

Comparing the development of alveolar bone and long bone

Previously to comparing long and alveolar bone, alveolar bone development stages were explored throughout tooth development stages of molar. At the bud stage, embryonic day 12 (E12), multiple mesenchymal stem cells beneath the tooth bud were condensed to form basal bone (Figure 10A). At the bud-to-cap transition, E14, mineralized bone was discovered around the site where basal bone usually forms. When enamel organ begins to form cervical loops, outer portion of the dental follicle which was positioned near the cervical loop started to form alveolar bone. (Figure 10B). At the cap to bell stage, E16 and E19, alveolar bone grew more actively near the developing tooth. Incisor began to be seen beneath the bone that covers the molar root. (Figure 10C, D, and E). At the hard tissue formation, postnatal day 7 (PN7), molar and incisor were almost fully covered by alveolar bone. Specifically, when the outer enamel epithelium approached the inner compartment of the enamel organ, the molar region alveolar bone almost fully covered the crown region (Figure 10F). At root formation stage, PN21, the majority of the bones were well matured, while small amounts of dental epithelial-derived tissues remained in the periodontal ligaments (Figure 10G).

Long bone was analyzed with femur, specifically the diaphysis region. At E12 and E14, most of the hind limbs were formed with cartilage (Figure 10H, I). At E16 and E19, diaphysis parts transformed to bone tissue (Figure 10J, K). At PN7, bone and marrow cavity became distinguishable (Figure 10L). At PN21, cortical bone and marrow cavity were well matured (Figure 10M). These data

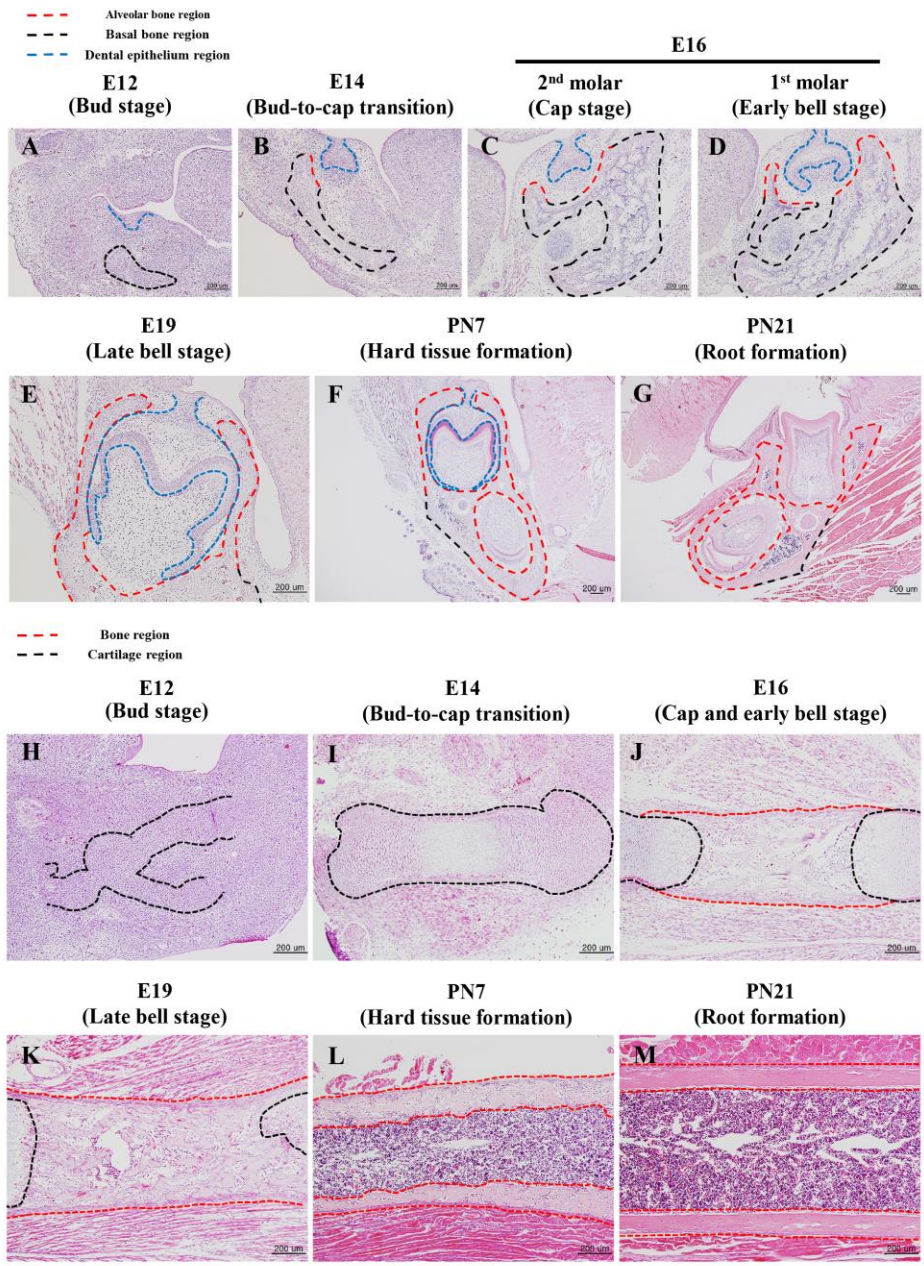

Figure 10. Alveolar bone and long bone development during mouse tooth development stage. (A, H) Embryonic day 12 (bud stage). (B, I) Embryonic day 14 (bud-to-cap transition). (C, D, J) Embryonic day 16 (2nd molar, cap stage (C) & 1st molar, early bell stage (D)). (E, K) Embryonic day 19 (late bell stage). (F, L)

Postnatal day 7 (hard tissue formation). (G, M) Postnatal 21 day (root formation). (A-G) The region covered by the red dashed line: alveolar bone. The region covered by the black dashed line: basal bone. (H-M) The region covered by the red dashed line: bone. The region covered by the black dashed line: cartilage. E, embryonic; PN, postnatal.

elucidate that alveolar bone development begins at the bud-to-cap stage and most actively formed at the hard tissue formation. Simultaneously, long bone was discovered to actively form at the same stage. During the development, epithelial tissue was located more closely and for a longer duration to alveolar bone than long bone.

Distinct characteristics of primary mouse alveolar bone and long bone-derived cells

To analyze the characteristics of each bone cell *in vitro*, I harvested bone cells from each tissue. Alveolar bone- and long bone-derived cells were isolated at hard tissue formation stage, when both bone formations were most active (Figure 10F, L). mABDC and mLBDC were explanted from each of the bone pieces, and their morphology looked similar (Figure 11A, B, C, and D). Proliferative activity was similar in both bone-derived cells (Figure 11E). To confirm their osteoblastic characteristic, I compared both bone-derived cells with non-osteogenic cells, specifically mouse primary dermal fibroblast (mDF) from the ventral skin. *Bsp* was highly expressed in both bone-derived cells when compared with mDF. Both bone-derived cells manifested mineralized nodule formation after osteogenic differentiation, but not in mDF (Figure 11F, G). These results indicate that mABDC and mLBDC have osteoblastic characteristics and similar proliferative activity and morphology.

To investigate whether the NC and EMI-related gene were differently regulated between two tissues, I measured the mRNA expression level of Msx and

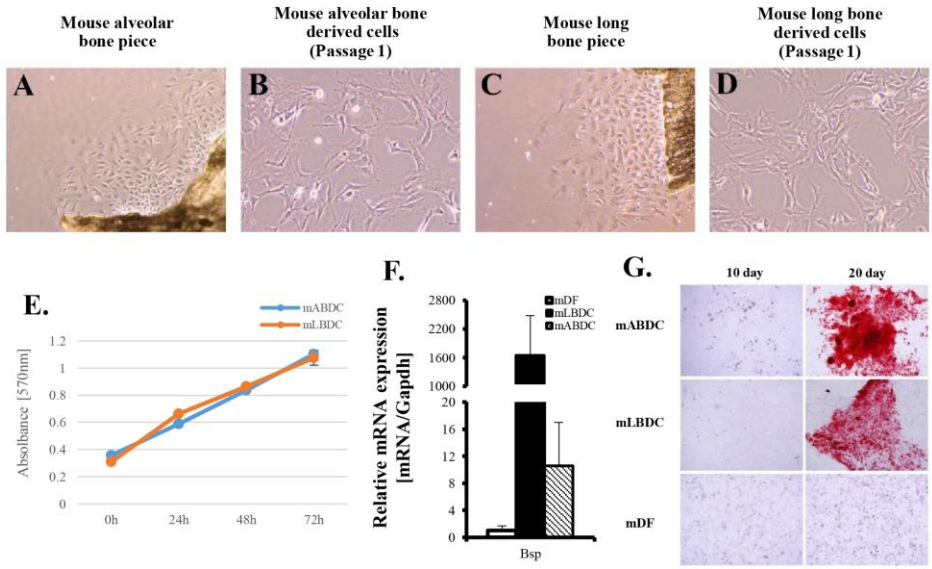

Figure 11. Characteristics of mouse alveolar bone and long bone derived cells. (A-D) Morphology of cells derived from alveolar bone and long bone. (A, B) Primary cultured cells isolated from alveolar bone pieces and passage 1 cells. (C, D) Primary cultured cells isolated from long bone pieces and passage 1 cells. Cells were observed under an optical microscope (X 100). (E) MTT assay was analyzed in both bone derived cells for 3 days. (F) Expression levels of osteoblast marker gene, Bsp, obtained by real-time PCR from cDNA of mABDC, mLBDC and mDF. Real-time PCR values are normalized to the internal housekeeping gene, Gapdh. (G) Alizarin Red S staining (ARS). Cells were cultured in osteogenic induction media for 10 and 20 days.

Bmp family, *Dlx5, Nfic*, and *Cpne7* genes in cells and tissues. The expression level of *Msx* and *Dlx* genes were higher in cell and tissue of alveolar bone than in long bone. Interestingly, the expression level of *Bmp, Nfic*, and *Cpne7* genes were not consistent between alveolar bone and long bone. Contrary to *Nfic* and *Cpne7*, *Bmp2* and *Bmp4* mRNA expressions were distinct in mABDC and mLBDC. However, the expression level of all EMI-related genes were higher in alveolar bone than long bone tissue (Figure 12A). The mineralization capacities were also different in mABDC and mLBDC. Mineralized nodule formation was more elevated in mLBDC than mABDC (Figure 12B). Therefore, I focused on gene expression at genome level to find the more evidence of different characteristics. The expression profiles between alveolar bone and long bone were compared using transcriptome sequencing data. The multidimensional scaling plot and heat map for hierarchical clustering showed the distinct transcriptome profile between mABDC and mLBDC (Figure 12C, D). Moreover, Gene ontology about biological process, molecular function, and cellular component, and KEGG pathway analysis for functional studies also showed different characteristics (Figure 13). To analyze the precise gene expression change, I focus on the classes of genes related to osteogenic differentiation, NC, and EMI. Most of osteogenic genes were more highly expressed in mLBDC than mABDC. NC and EMI- related genes showed consistent pattern between two types of bone cells (Figure 12E). To verify the origin of bone, the cranial neural crest cells and derivative marker expression were also analyzed (Figure 14). These results indicate that gene expression profiles of alveolar bone and long bone are different. Alveolar bone express higher levels of NC-related genes than long bone. Meanwhile, EMI-related gene expression profiles were different between the two different bones, both in cellular and tissue

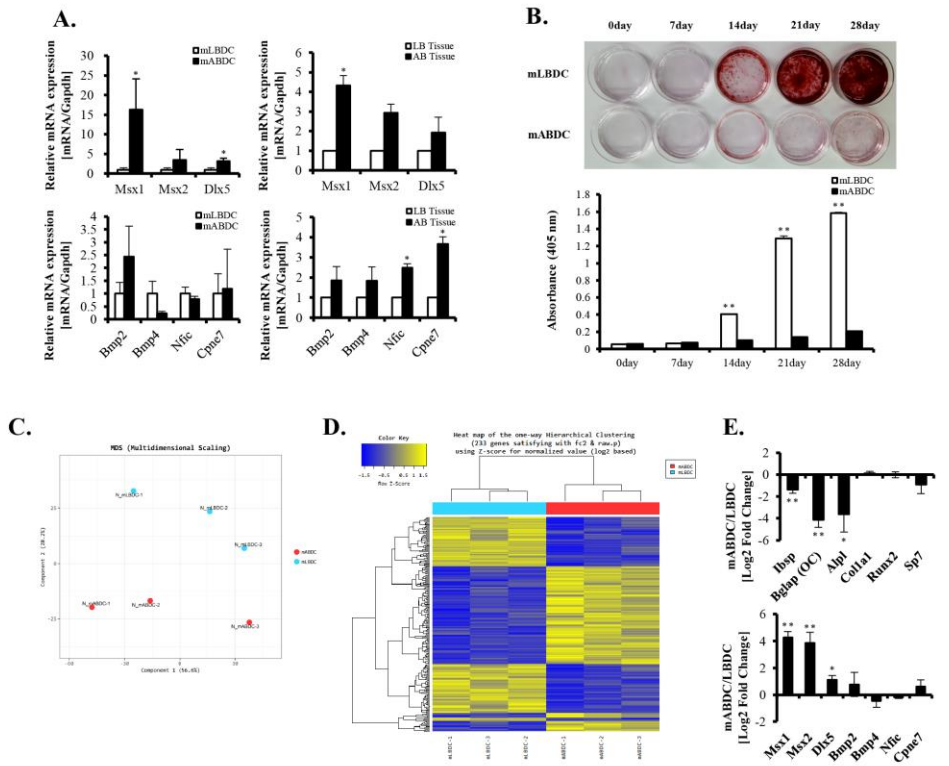

Figure 12. Characteristics of alveolar bone and long bone. (A) NC and EMI-related gene expression of confluent, primary cultured mouse bone-derived cells, and bone tissues analyzed by qPCR. All values are normalized to the Gapdh. (B) ARS in both bone-derived cells during osteogenic differentiation for 28 days. (C–E) Comparing expression profiles between mABDCs and mLBDCs using transcriptome sequencing data. (C) Multidimensional scaling plot. (D) Heat map for hierarchical clustering. (E) Relative gene expressions from set of osteogenic, NC, and EMI-related genes. Sequencing data analyzed from triplicated RNA sequencing data of mABDC and mLBDC samples. AB tissue = alveolar bone tissue; Alpl = alkaline phosphatase; ARS = Alizarin Red S staining; Bglap = osteocalcin; Dlx = distal-less homeobox; Bmp = bone morphogenetic protein;

Cpne7 = copine-7; EMI = epithelial–mesenchymal interaction; Ibsp = bone sialoprotein; LB tissue = long bone tissue; mABDCs = mouse alveolar bone-derived cells; mLBDCs = mouse long bone-derived cells; Msx = msh homeobox; NC = neural crest; Nfic = nuclear factor I-C; Runx2 = runt-related transcription factor 2; Sp7 = osterix; Col1a1 = collagen type I alpha 1 chain. All statistical analysis performed by Student's t test, n = 3, $*p < 0.05$, $**p < 0.005$.

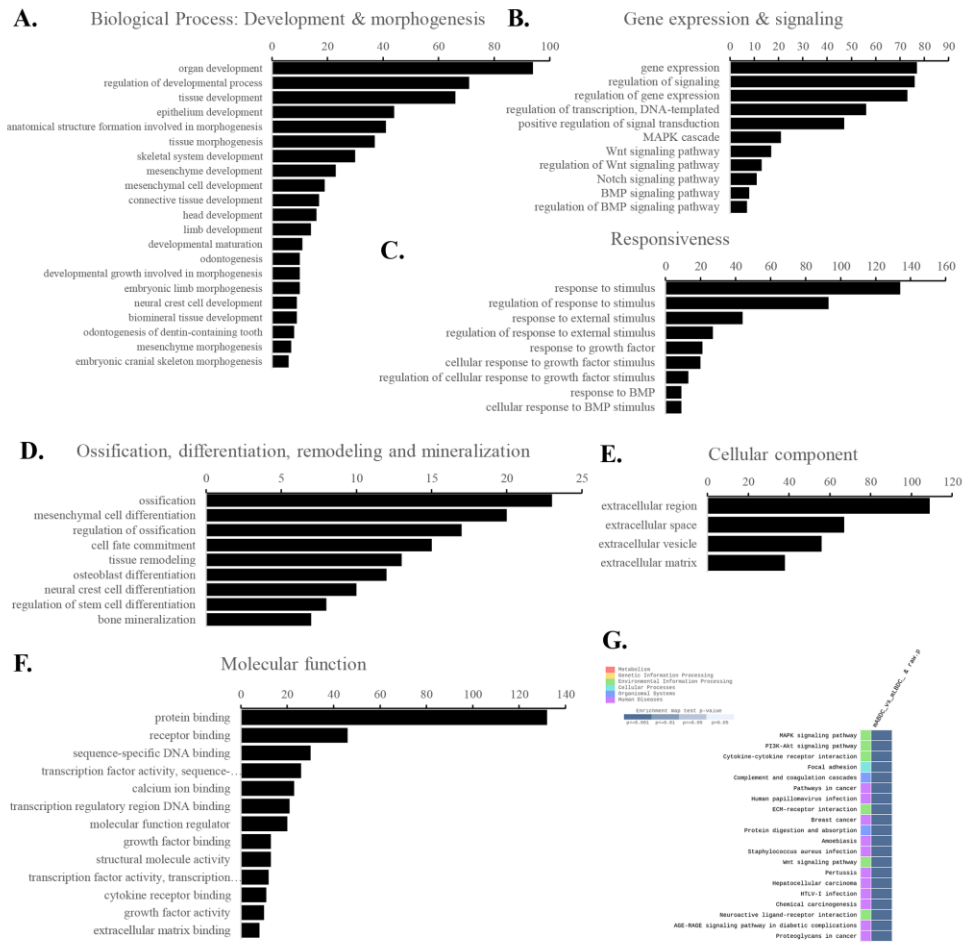

Figure 13. Functional analysis of RNA sequencing data. (A-F) Bar plot of gene-enrichment and functional annotation analysis using gene ontology. (A-D) Terms of biological process category. (A) Development and morphogenesis-related terms (B) Gene expression and signaling-related terms. (C) Responsiveness-related terms. (D) Ossification, differentiation, remodeling, and mineralization-related terms. (E) Terms of molecular function category. (F) Terms of cellular component category. (G) Top 20 terms in enrichment test of KEGG pathway analysis.

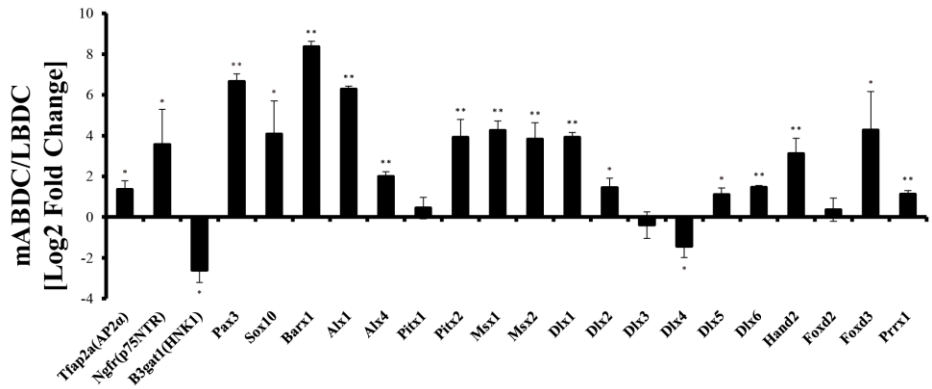

Figure 14. Relative mRNA expression of CNC-related genes. Relative expression of genes expressed in craniofacial NC cells, NC-derived craniofacial/ pharyngeal arch mesenchyme, craniofacial skeleton, limb bud mesenchyme. Those genes are known as markers of neural crest stem cell, NC progenitor cell, and craniofacial neural crest cell. All statistical analysis performed by Student t-test, n = 3, $*p < 0.05$, $**p < 0.005$.

level.

To compare the gene regulation in mABDC and mLBDC during osteogenic differentiation, I analyzed mRNA expression patterns of osteogenic, NC, and EMI-related genes during osteogenic differentiation. *Bsp, OC* and *Bmp2* showed continuously increased expression patterns in both. Meanwhile, NC-related genes, EMI-related genes, and *Alp* showed different expression patterns between mABDC and mLBDC. In mLBDC, the expression pattern of the genes gradually increased during early differentiation and decreased during late differentiation. In mABDC, however, the expression progressively increased during differentiation. Only *Msx2* expression gradually decreased during early differentiation and increased during late differentiation (Figure 15A, B, and C). Protein expression levels showed consistently different patterns, excluding DLX5 (Figure 15D). These data could suggest that gene expression in mABDC and mLBDC were different during osteogenic differentiation.

Different effects of dental epithelial secreted proteins in mABDC and mLBDC

I found different expressions of osteogenic and EMI-related genes in mABDC and mLBDC. To find the effect of EMI on other genes – especially in alveolar bone – I treated EMI-related protein, which is known to be secreted from dental epithelium, to mABDC and mLBDC. I analyzed mRNA expression levels of the osteogenic, NC, and EMI-related genes after protein treatment. Expression of most osteogenic genes were elevated in both bone-derived cells in the BMP4

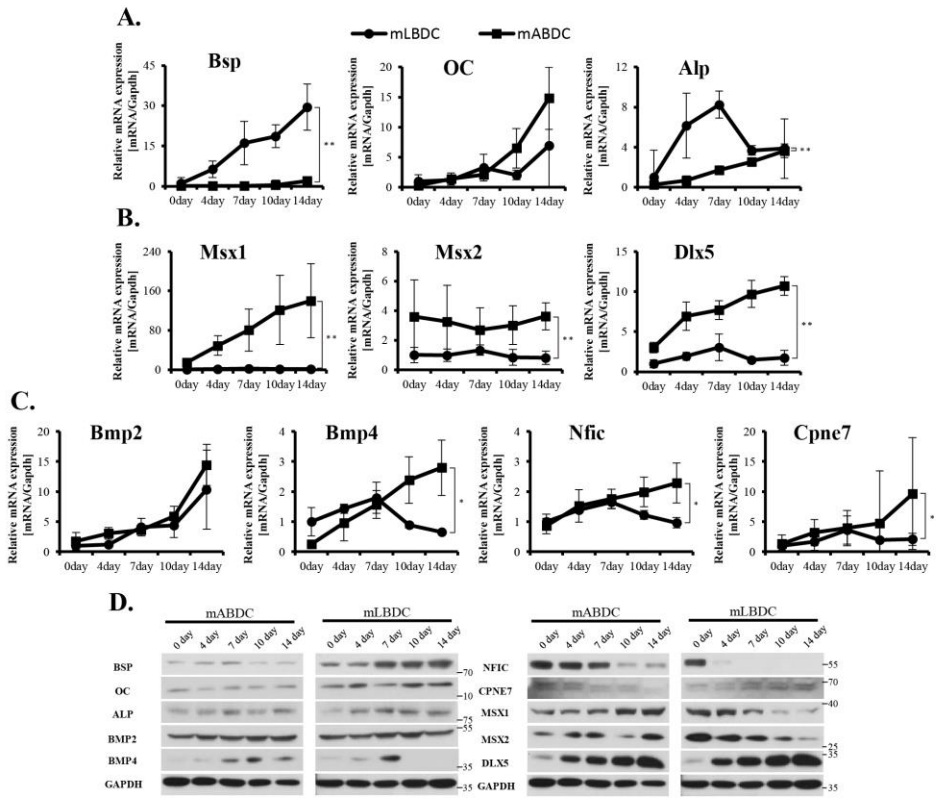

Figure 15. Expression levels of osteogenic, NC, and EMI-related genes during osteogenic differentiation in mLBDCs and mABDCs. (A) Osteogenic genes, Bsp, OC, and Alp expression levels observed during differentiation. (B) NC-related genes, Msx1, Msx2, and Dlx5 expression levels observed during differentiation. (C) EMI-related genes, Bmp family, Nfic, and Cpne7 expression levels observed during differentiation. Real-time PCR values are normalized to the Gapdh. (D) All values were also evaluated by protein expression level. GAPDH was used as internal control. Molecular weight markers were mentioned beside. Differentiation of mLBDCs and mABDCs for 14 days and analyzed by qPCR and Western blot. Bsp = bone sialoprotein; Alp = alkaline phosphatase; Dlx = distal-less homeobox; Bmp = bone morphogenetic protein; Cpne7 = copine-7; EMI = epithelial–

mesenchymal interaction; mABDCs = mouse alveolar bone-derived cells; mLBDCs= mouse long bone-derived cells; Msx = msh homeobox; Nfic = nuclear factor I-C; OC = osteocalcin. All statistical analysis performed by two-way ANOVA, n =3, *$p < 0.05$, **$p < 0.005$.

treatment group, except *OC* which only elevated in mABDC. In BMP4 treated groups, rate of increase in most osteogenic genes expressions was higher in mABDC than mLBDC. Meanwhile, *Runx2* was more elevated in mLBDC (Figure 16A). NC-related genes, *Msx2* and *Dlx5*, were upregulated in BMP4 treatment group (Figure 16B). EMI-related genes showed diverse results. *Bmp2* was highly elevated in BMP4 treated group. But Bmp4 was downregulated in BMP4 treated groups. *Nfic* expression showed opposite effects of BMP4 in each cell. *Cpne7* expression was slightly repressed in all protein treated groups (Figure 16C). These data indicate that BMP4 regulates most osteogenic and NC-related genes more than CPNE7 in both bone-derived cells. The effects seemed more efficient in mABDC than in mLBDC.

BMP4 showed a more dynamic effect in bone-derived cells from the different EMI-related secretion proteins from epithelial tissue. Specially, *Msx2* and *Dlx5* were also affected by that protein. To investigate whether BMP4 regulates genes during osteogenic differentiation, respectively in mABDC and mLBDC, I analyzed mRNA expression in cells. In mABDC, osteogenic genes were elevated in BMP4 treated groups during early differentiation stages. Late osteogenic markers, *OC*, *Osx*, and *Dmp1*, also showed higher expression in BMP4 treated group than in control group. In BMP4 treated mLBDC, all of the osteogenic genes were downregulated, but *Bsp* was upregulated during differentiation. Even, the rate of increase in *Bsp* expressions was higher in BMP4 treated mABDC than mLBDC (Figure 17A). Some NC and EMI-related genes, *Msx2* and *Dlx5*, were also highly expressed in both BMP4 treated mABDC. mRNA expression pattern of *Dlx5* was downregulated during late osteogenic differentiation in BMP4 treated groups.

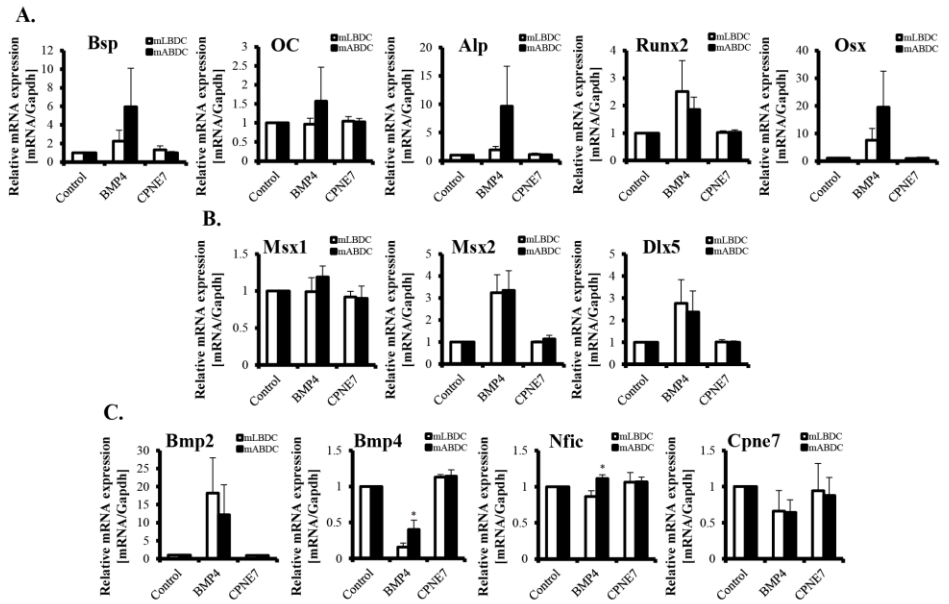

Figure 16. Expression levels of osteogenic, NC, and EMI-related genes in mLBDCs and mABDCs after EMI-related proteins treatment. (A) Expression levels of osteogenic genes. (B) Expression levels of NC-related genes. (C) Expression levels of EMI-related genes. Real-time PCR values are normalized to the Gapdh. Cells were treated with 100 ng/mL proteins for 48 hours and analyzed by qPCR. Bsp = bone sialoprotein; Alp = alkaline phosphatase; Dlx = distal-less homeobox; Bmp = bone morphogenetic protein; Cpne7 = copine-7; EMI = epithelial–mesenchymal interaction; mABDCs = mouse alveolar bone-derived cells; mLBDCs= mouse long bone-derived cells; Msx = msh homeobox; Nfic = nuclear factor I-C; OC = osteocalcin; Osx = osterix; Runx2 = runt-related transcription factor 2. All statistical analysis performed by Student's t test, n = 3, $*p < 0.05$.

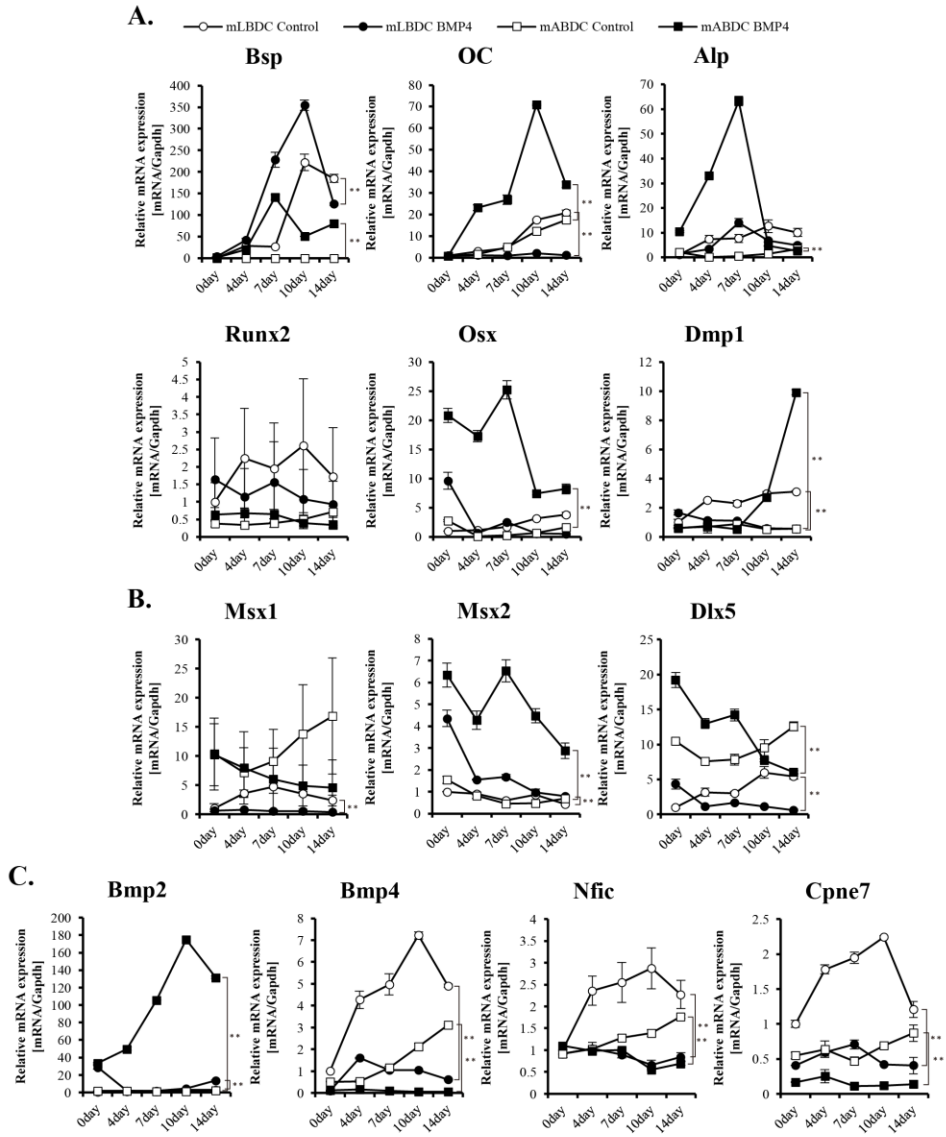

Figure 17. Expression levels of osteogenic, NC, and EMI-related genes in BMP4-treated mLBDCs and mABDCs during osteogenic differentiation. (A) Expression levels of osteogenic genes. (B) Expression levels of NC-related genes. (C) Expression levels of EMI-related genes. Real-time PCR values are normalized to the Gapdh. Cells were treated with 100 ng/mL BMP4 proteins during differentiation and analyzed by qPCR. Bsp = bone sialoprotein; Alp = alkaline phosphatase; Dlx = distal-less homeobox; Bmp = bone morphogenetic protein;

Cpne7 = copine-7; EMI = epithelial–mesenchymal interaction; mABDCs = mouse alveolar bone-derived cells; mLBDCs= mouse long bone-derived cells; Msx = msh homeobox; Nfic = nuclear factor I-C; OC = osteocalcin; Osx = osterix; Runx2 = runt-related transcription factor 2; Dmp1 = dentin matrix protein 1. All statistical analysis performed by two-way ANOVA, n = 3, *$p < 0.05$, **$p < 0.005$.

Similar downregulated patterns were found in other osteogenic genes in mABDC (Figure 17B). In EMI-related genes, *Bmp2* was extremely elevated; however, *Bmp4* was downregulated in both BMP4 treated cells similarly to the non-differentiated status results. Both *Nfic* and *Cpne7* were suppressed during osteogenic differentiation in BMP4 treated groups (Figure 17C). These results demonstrate that BMP4 significantly induces osteogenic and NC-related genes in mABDC than mLBDC during differentiation.

BMP4 elevates alveolar bone formation more than long bone formation

To determine the role of BMP4 in osteogenic differentiation and bone formation *in vivo*, I transplanted mABDC and mLBDC into subcutaneous tissues of immunocompromised mice in the presence of hydroxyapatite/tricalcium phosphate (HA/TCP) under four different conditions: mABDC-only, mLBDC-only, mABDC with rBMP4, and mLBDC with rBMP4. Six weeks after transplantation, bone like tissues were formed at the periphery of HA/TCP particles only in BMP4 treated groups. The rBMP4-treated mABDC group exhibited more bone like tissues than the rBMP4-treated mLBDC group. Contrastingly, marrow-like tissue including adipose tissue presented an opposite response. These phenomenon was more prominent after twelve weeks (Figure 18A, B). Protein expression of BSP, which known as a typical bone marker, was higher in the mLBDC-only group than the mABDC-only group. Contrarily, mABDC expressed more BSP protein than mLBDC in rBMP4 treated group (Figure 18C). Osteoclast number was increased in both BMP4-treated groups (Figure 19). These results confirm that bone formation

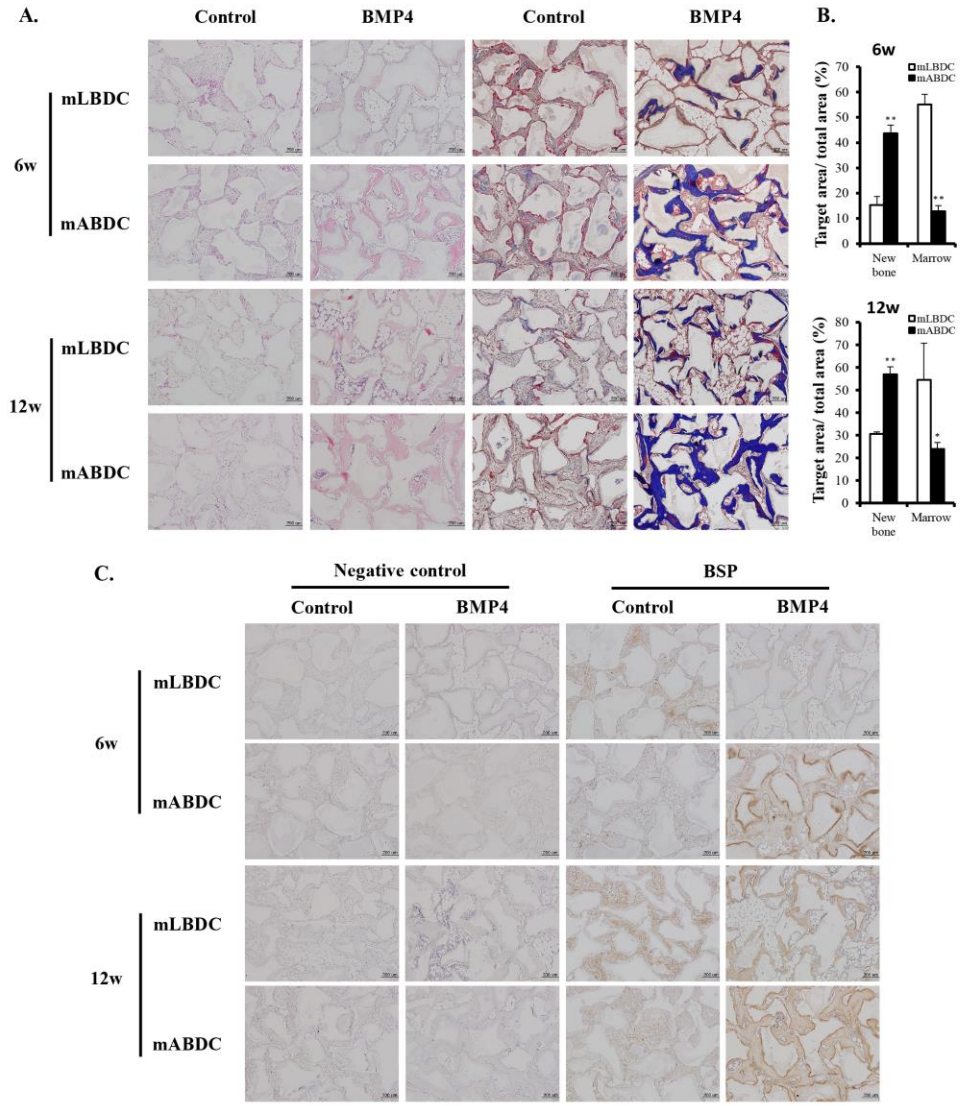

Figure 18. Histological analysis of the regenerated bone matrix using mABDCs and mLBDCs *in vivo*. The mouse bone-derived cells were mixed with 100 mg HA/TCP particles alone, or with BMP4 in a 0.5% fibrin gel and transplanted s.c. into immunocompromised mice for 6 and 12 weeks. (A) Samples were stained with H&E and Masson's trichrome. (B) Quantification of mineralized matrix and marrow-like space at 6 and 12 weeks. (C) Mineralized tissues were immunostained with anti-bone sialoprotein. Negative control only stained by

second rabbit antibody. HA/TCP = Hydroxyapatite/tricalcium phosphate; mABDCs = mouse alveolar bone-derived cells; mLBDCs = mouse long bone-derived cells. All statistical analysis performed by Student's t test, n = 3, *$p < 0.05$, **$p < 0.005$.

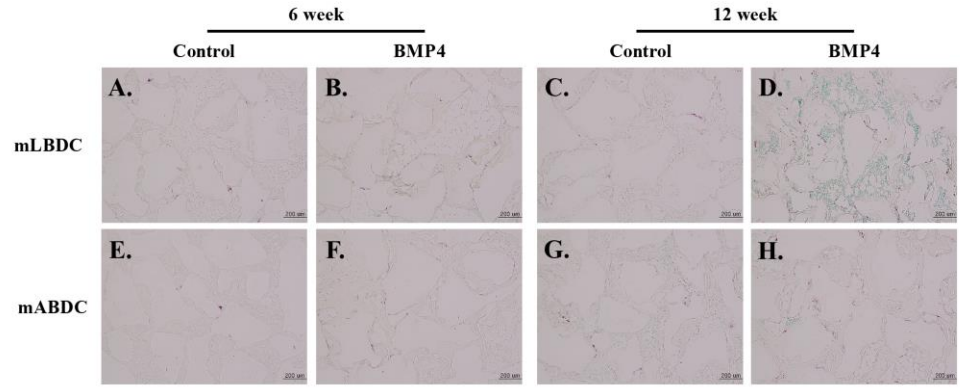

Figure 19. Histological analysis of the osteoclast using mABDC and mLBDC *in vivo*. Samples were stained with TRAP (Tartrate-resistant acid phosphatase) (A-D) mLBDC. (E-H) mABDC.

capacity of BMP4 is greater in mABDC than mLBDC *in vivo*.

IV. DISCUSSION

Alveolar bone is a component of the periodontium tissue which is formed by the ectomesenchyme-derived dental follicle cell. Some studies reveal that the interaction of ectomesenchyme and dental epithelium is essential during periodontium development, the same goes for tooth development (Cho and Garant, 2000). Previous studies mention about the beginning stages of mouse alveolar bone formation (Zhang et al., 2003). However, the development stages of alveolar bone is not defined in detail (Lee et al., 1992; Kronenberg, 2003; Blumer et al., 2007; Lungova et al., 2011; Jia et al., 2013). For better analysis, the stages were outlined using the tooth development stages as a guide. Along with these stages, to compare long to alveolar bone, this study performed a histological analysis. During this analysis, I observed that epithelial tissue was located more closely and for a longer duration to developing alveolar bone than long bone. These observations infer that alveolar bone formation could be associated with dental epithelium conformational changes. Overall, alveolar bone development could be more related to epithelial tissue than long bone development.

To exclude as many confounding factors, I harvested mLBDC from the diaphysis region of the long bone for comparison. There are two kinds of ossification during bone development: intramembranous and endochondral (Long and Ornitz, 2013). Most craniofacial bones are formed via intramembranous ossification. Long bone is created by endochondral ossification. However, when perichondrium transforms to periosteum, osteoblasts form new bone beneath the perichondrium with intramembranous ossification at the diaphysis region (Mundlos and Olsen, 1997; Lanske et al., 1999). By selecting a similarly intramembranous

ossified bone, I limited the confounding factors that could arise from comparing differently ossified bone. Anatomically, human mandible bone consists of alveolar bone, basal bone, and cartilaginous processes. On the other hand, the mouse mandible consists of the alveolar region and ascending ramus, including coronoid, condylar, and angular processes (Klingenberg et al., 2001). Most of the alveolar region is derived from neural crest cells, whereas ascending ramus has the non-neural crest-derived mesenchymal cells also (Aggarwal et al., 2010). In order to control any confounding variables that can arise from comparing two different developmental origins, I harvested bone at the alveolar process region only.

To compare alveolar bone to long bone, NC, and EMI-related genes in primary cultured bones between alveolar bone and long bone were analyzed. Primary cultured bone cells showed different characteristics between alveolar bone and long bone in NC and EMI-related gene expression. Homeobox genes – *Msx* family – are abundant in mesenchymal NC cells in pharyngeal arches and craniofacial skeleton (Ishii et al., 2005). When mutated, mouse exhibited absence and/or malformation of alveolar bone (Satokata and Maas, 1994; Aioub et al., 2007). Another NC-related gene, *Dlx* family genes, also plays a significant role in embryonic development and is seen expressed in cranial neural crest-derived craniofacial primordia and limbs. The lack of functional *Dlx5* in mice results in dysmorphogenesis in almost all cranial bones including incisive and molar alveolar bone (Depew et al., 1999). However, for limbs, single homozygous mutants of *Msx1*, *Msx2*, and *Dlx5* do not display gross abnormalities (Robledo et al., 2002; Lallemand et al., 2005). As hinted, NC-related are known as regulators of EMI during orofacial and limb developments (Bendall and Abate-Shen, 2000). NC-

related genes were more highly expressed in alveolar bone tissue and cells than in long bone. Also, their expressions were higher in mABDC than mLBDC during differentiation. These results hint that abundant expression of NC-related genes could be a marker for alveolar bone. I theorized that EMI would affect alveolar bone more than long bone due to EMI being strongly regulated from the abundant expression of NC-related genes.

Previous studies have explored EMI and *Bmp2*, *Bmp4*, *Nfic*, or *Cpne7* individually in either alveolar or long bone. In this study, I look at these individual relationships as a group and attempt to understand how these relationships fit in the bigger picture of how correlated or different alveolar and long bone are. *Bmp* was selected for our analysis because Bmp signaling is crucial for regulating EMI during organogenesis – organs formed include tooth and limb (Jones et al., 1991; Niswander and Martin, 1993). Specifically, *Bmp2* and *Bmp4* are frequently codistributed, and their expression shifts between epithelium and mesenchyme (Thesleff and Mikkola, 2002). Along with *Bmp*, *Nfic* was also observed because a previous study defined it as a component of EMI in ectomesenchyme (Huang et al., 2010). *Nfic* knock-out mice showed defective alveolar bone formation and osteoporosis like phenotype in long bone (Steele-Perkins et al., 2003; Lee et al., 2014a). Finally, *Cpne7* was explored between the two because it is secreted from dental epithelium, and effects on odontogenic induction to dental mesenchyme was confirmed in a previous study (Lee et al., 2011b; Oh et al., 2015). While previous studies merely confirmed the existence of EMI in alveolar and long bone, this study illustrated distinct EMI-related gene expression patterns in alveolar bone and long bone. Upon seeing the expression patterns, I inferred that the regulation of

EMI in alveolar bone and long bone could be different.

Along with the differences seen NC and EMI-related genes, a difference in mineralization capacity was seen between long and alveolar bone. Mineralization capacity was more elevated in mLBDC than mABDC. In contrast, their morphology and proliferation rate were not significantly different. These results aligned with osteogenic gene expression patterns in mLBDC through RNA-seq. Interestingly, a different study showed a more elevated mineralization capacity in mABDC than mLBDC (Aghaloo et al., 2010). This discrepancy is thought to result from the different bone cell harvesting method. The other study used primary bone marrow cells, while I used primary cells from the bone surface.

As mentioned above, although initially inferred, alveolar and long bone showed distinct genetic profiles. Specifically, osteogenic, EMI, and NC-related genes were different in mABDC and mLBDC. To confirm these results, RNA sequencing was used, and the difference between mABDC and mLBDC's EMI and NC-related gene expression was confirmed. Along with the differences seen during standard conditions, EMI and NC-related gene expression patterns were also different during osteogenic differentiation. Considering how most NC-related genes are known as transcription factors that regulate osteogenic gene expression, these results hint that different regulation of EMI and NC-related genes take part in altering bone characteristics to result either in alveolar or long bone (Nelms and Labosky, 2010).

To further compare alveolar and long bone, their osteogenic, NC-related, and EMI-related gene responsiveness to developing dental epithelial secretions were compared. The responsiveness to developing dental epithelial secretions were

selected because they induce differentiation of mesenchyme cells through gene regulation (Thesleff et al., 1995). To compare the effects, I analyzed gene expression in BMP4 and CPNE7 treated mABDC and mLBDC. To recap, despite their correlation as EMI-related genes, MSX1, MSX2, DLX5, and NFIC were not treated because they are transcription factors inferred to not be secreted from dental epithelial cells.

Initially, osteogenic gene responsiveness to developing dental epithelial secretions was compared between alveolar and long bone. From BMP4 and CPNE7, BMP4 treated cells illustrated a stronger regulation of osteogenic genes. BMP4 elevated mRNA expression of osteogenic genes in mABDC. However, for BMP4 treated mLBDC, *OC* was not regulated. Relatively to mLBDC, *Bsp, Alp,* and *Osx* were more elevated in mABDC. During differentiation, most osteogenic genes were downregulated in BMP4-treated mLBDC. *Bsp* increased in both mABDC and mLBDC. The increment of increase in mABDC after the BMP4 treatment was greater than the magnitude of increase in mLBDC after the treatment. In the *in vivo* model – contrary to the cell only group – BMP4-treated mABDC group formed more BSP positive bone-like tissue than BMP4-treated mLBDC. Another osteogenic gene and osteocyte marker, *Dmp1*, was upregulated in BMP4-treated mABDC at the late stages of differentiation. In mLBDC, *Dmp1* was downregulated in mLBDC during the entire differentiation stage. In the *in vivo* study, masson's trichorome stained tissue showed a more mature bone-like matrix in BMP4-treated mABDC group than the BMP4-treated mLBDC group. Overall, our findings indicate that BMP4 could accelerate the maturation of alveolar bone by stimulating *Dmp1*; this effect was not seen in long bone. Our results provide that the BMP4

induce more bone formation and maturation in alveolar bone than in long bone by upregulating osteogenic genes.

Following osteogenic gene comparison, the NC-related gene responsiveness to developing dental epithelial secretions was compared. BMP4, along with the osteogenic genes, was seen to upregulate NC-related genes, *Msx2* and *Dlx5*, in both cells. *Msx2* gene expression – expressed in mandibular alveolar bone during skeletal growth – was elevated in response to BMP4 during osteogenic differentiation (Aioub et al., 2007). Previous studies show *Msx2* inducing *Alp* activity and inhibiting adipogenesis by diminishing the expression of *Pparγ* (Ichida et al., 2004). Again, when treated with BMP4, *Dlx5* was upregulated in mABDC during the early stages of differentiation. Whereas, for mLBDC, *Dlx5* was downregulated during the entire differentiation stage. There was no change in the other NC-related gene, *Msx1*. In the *in vivo* model, volume of marrow-like tissue including adipose tissue was smaller in BMP4-treated mABDC than BMP4-treated mLBDC. BMP4 regulates alveolar bone formation in *Msx1* knock out mouse via inducing *Dlx5* and *Runx2* expression (Zhang et al., 2003). These results suggest that BMP4 induces alveolar bone-specific bone formation by regulating *Msx2* and *Dlx5* expression. Furthermore, while previous studies show that *Msx1* has an effect on BMP4 in alveolar bone, our results show that BMP4 doesn't affect *Msx1*, inferring a downstream relationship (Zhao et al., 2000). Finally, our results show that elevated levels of *Msx2* could also affect the proportion of marrow tissue in bone.

Finally, for the comparison, EMI-related gene responsiveness to developing dental epithelial secretions was observed. The responsiveness that were

immediately noticed were *Cpne7*, *Bmp2*, and *Bmp4*. For CPNE7, I observed that CPNE7 did not regulate any genes in mABDC and mLBDC. *Cpne7* was observed to be downregulated by BMP4 in both bone-derived cells during differentiation. These observations infer that *Cpne7* may have a distinct function in odontogenic cells and osteogenic cells. *Bmp2* is the most well-known bone-inducing factor. Interestingly, BMP4 induced *Bmp2* expression in both cells. Rate of increase of *Bmp2* induced by BMP4 was higher in mABDC than in mLBDC during differentiation. *Bmp4* expression was downregulated in both BMP4-treated cells. Based on these results, I infer the possibility of BMP4 induced bone formation effects resulting from BMP4 upregulating *Bmp2*, which then affects bone formation. Furthermore, I speculate that the effects of BMP4 could be controlled by negative feedback.

While observing the differences between alveolar and long bone, I discovered epithelium and BMP4 potentially affecting alveolar bone. To confirm the previous data regarding NC and EMI-related gene differences between the two bones, RNA sequencing was performed. When the sequencing was executed, significant differences between the two bones were observed as the following: BMP pathways, BMP responsiveness, odontogenesis, epithelium, and mesenchyme. When the osteogenic gene responsiveness was observed, I saw that BMP4 elevated the mRNA expression of osteogenic genes in mABDC. Furthermore, when the cell was BMP4 treated, I observed that the rate of increase of *Bsp* was higher in mABDC than mLBDC during differentiation. Regarding the NC-related gene responsiveness, I saw that BMP4 controlled *Msx2* and *Dlx5* in mesenchyme cells although the origin of BMP4 (epithelium or mesenchyme) is unknown BMP4

seems to be specifically significant in mABDC osteogenic growth, considering how there was a drastic change in EMI-related gene responsiveness. Overall, once again, EMI-related gene responsiveness showed that BMP4 could play a significant role in mABDC by having a steeper increase of BMP4 induced *Bmp2* in mABDC than mLBDC during differentiation (Figure 20). Our findings line up with a previous study that reveals that *Bmp4* knockout in epithelial cells had a more severe effect on alveolar bone than the knockout in mesenchyme cells (Liu et al., 2005; Jia et al., 2013). When the damage was compared between alveolar and long bone, the study revealed that damage in alveolar bone was more severe – at times, long bone showed no defect (Tsuji et al., 2008; Maatouk et al., 2009).

In summary, I elucidated the different genetic profiles of alveolar bone and long bone. Additionally, EMI-related epithelial factor, BMP4, was seen to affect alveolar bone formation more than long bone by regulating the expression of osteogenic, EMI, and NC-related genes. By detailing the differences between alveolar and long bone, the present study emphasizes the need of tissue specific bone treatment. This can be seen from the different gene responses for BMP4 in long and alveolar bone. More specifically, based on our results, this study highlights the need of a distinct treatment specifically for alveolar bone, considering how distinctly different the bone is.

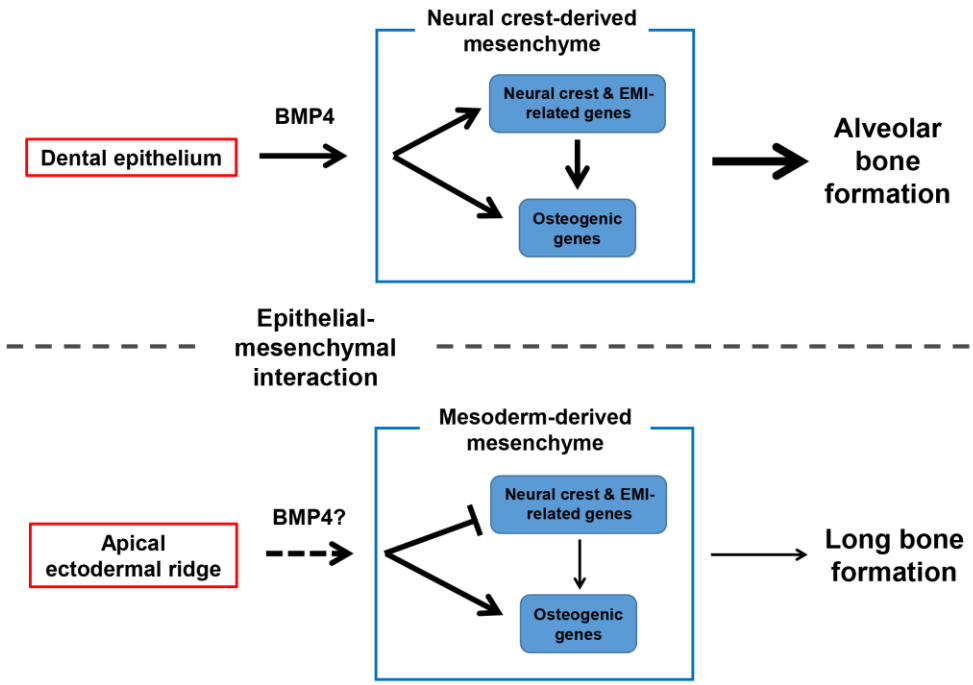

Figure 20. Schematic illustration of the different responsiveness of alveolar and long bone to EMI-related factor, BMP4. Both alveolar bone and long bone development are associated with epithelial-mesenchymal interaction (EMI). However, different factors secreted from each epithelium affect adjacent mesenchyme sequential and reciprocal manner respectively. BMP4, the dental epithelium factor, accelerated the expression of neural crest and EMI-related genes in neural crest-derived mesenchyme, while it rather inhibited the expressions in mesoderm-derived mesenchyme. Indeed, osteogenic genes were markedly upregulated in BMP4-treated neural crest-derived mesenchyme than in mesoderm-derived mesenchyme. In all, the distinct gene regulation by BMP4 brought the phenomenon where the alveolar bone formation was massive than long bone formation.

CHAPTER IV. CONCLUDING REMARKS

In these studies, 1) the underlying mechanisms involved in tubular dentin formation of CPNE7 and 2) different responsiveness of alveolar bone and long bone were investigated.

In the beagle tooth defect model, CPNE7 showed tubular dentin formation, whereas it was not observed in control. *In vitro* studies showed that DSP and LC3 II exhibited similar expression patterns during odontogenic differentiation, and indeed, autophagy was induced by CPNE7 in pre-odontoblasts and mature odontoblasts. Upon these findings, I speculated that functional retardation of mature odontoblast could be derived with decreased CPNE7 expression. Similarly, when CPNE7 is introduced in mature odontoblast, it would restore its functional activity. To examine these speculations, I found that mineralization and dentin formation of mature odontoblast was promoted through CPNE7-activated autophagy. Also, the physiological odontoblast process, which showed TAU-positive, elongated in rCPNE7-treated odontoblasts. Furthermore, CPNE7-induced autophagy clearly removed lipofuscin in mature odontoblasts. CPNE7-treated mouse tooth defect model showed physiological dentin regeneration *in vivo*. Although rapamycin significantly induced autophagy, it could not restore sufficient cellular activity of mature odontoblast. Interestingly, CPNE7 induced autophagy and simultaneously phosphorylated mTOR in mature odontoblast; on the contrary, rapamycin inhibited the phosphorylation of mTOR. These results hint that CPNE7 regenerates physiological dentin through proper reactivation of cellular function in mature odontoblast by inducing autophagy in a different way of rapamycin.

During the development of alveolar bone and long bone, they showed different aspects in regard of distance from mesenchymal to epithelial tissues and duration of which epithelial and mesenchymal tissues are closely located. Dental epithelial tissues seemed more related to developing alveolar bone than apical ectodermal ridge to developing long bone. Gene expression profile and mineralization capacity were different in mABDC and mLBDC. Especially, expressions of osteogenic markers, NC, and EMI-related genes were distinct in mABDC and mLBDC. Additionally, these genes also showed distinct expression patterns during osteogenic differentiation. Through these observations, I assumed that each characteristic of alveolar bone and long bone could be derived from distinct gene expression regulation via different aspects of EMI. Among the EMI-related factors secreted from dental epithelium, BMP4 elevated the expression of several osteogenic genes, Msx2, Dlx5, and Bmp2. mABDC showed drastic upregulation of these genes in response to BMP4 during osteogenic differentiation, while mLBDC showed an opposite manner. Furthermore, massive alveolar bone formation was observed in the recombinant BMP4-treated group compared to the long bone *in vivo*. My results revealed that alveolar bone and long bone have different responsiveness to EMI by distinct gene regulation.

Collectively, these studies provide evidences of 1) the underlying mechanisms of CPNE7-mediated physiological dentin regeneration and 2) different responsiveness to BMP4 in alveolar bone and long bone for tooth and periodontal treatment. Together, primary research and clinical application could cooperate to bring progress in the quality of life in elderly people.

REFERENCES

Aggarwal, V.S., Carpenter, C., Freyer, L., Liao, J., Petti, M., and Morrow, B.E. (2010). Mesodermal Tbx1 is required for patterning the proximal mandible in mice. *Dev Biol* 344(2), 669-681. doi: 10.1016/j.ydbio.2010.05.496.

Aghaloo, T.L., Chaichanasakul, T., Bezouglaia, O., Kang, B., Franco, R., Dry, S.M., et al. (2010). Osteogenic potential of mandibular vs. long-bone marrow stromal cells. *J Dent Res* 89(11), 1293-1298. doi: 10.1177/0022034510378427.

Aioub, M., Lezot, F., Molla, M., Castaneda, B., Robert, B., Goubin, G., et al. (2007). Msx2 -/- transgenic mice develop compound amelogenesis imperfecta, dentinogenesis imperfecta and periodental osteopetrosis. *Bone* 41(5), 851-859. doi: 10.1016/j.bone.2007.07.023.

Al-Bari, M.A.A., and Xu, P. (2020). Molecular regulation of autophagy machinery by mTOR-dependent and -independent pathways. *Ann N Y Acad Sci* 1467(1), 3-20. doi: 10.1111/nyas.14305.

Arana-Chavez, V.E., and Massa, L.F. (2004). Odontoblasts: the cells forming and maintaining dentine. *Int J Biochem Cell Biol* 36(8), 1367-1373. doi: 10.1016/j.biocel.2004.01.006.

Bendall, A.J., and Abate-Shen, C. (2000). Roles for Msx and Dlx homeoproteins in vertebrate development. *Gene* 247(1-2), 17-31. doi: 10.1016/s0378-1119(00)00081-0.

Bleicher, F. (2014). Odontoblast physiology. *Exp Cell Res* 325(2), 65-71. doi: 10.1016/j.yexcr.2013.12.012.

Blumer, M.J., Longato, S., Schwarzer, C., and Fritsch, H. (2007). Bone development in the femoral epiphysis of mice: the role of cartilage canals and the fate of resting chondrocytes. *Dev Dyn* 236(8), 2077-2088. doi: 10.1002/dvdy.21228.

Bosshardt, D.D., Stadlinger, B., and Terheyden, H. (2015). Cell-to-cell communication--periodontal regeneration. *Clin Oral Implants Res* 26(3), 229-239. doi: 10.1111/clr.12543.

Brudevold, F., Steadman, L.T., and Smith, F.A. (1960). Inorganic and organic components of tooth structure. *Ann N Y Acad Sci* 85, 110-132. doi: 10.1111/j.1749-6632.1960.tb49951.x.

Brunk, U.T., and Terman, A. (2002). Lipofuscin: mechanisms of age-related accumulation and influence on cell function. *Free Radic Biol Med* 33(5), 611-619. doi: 10.1016/s0891-5849(02)00959-0.

Chen, C.L., Chen, Y.H., Liang, C.M., Tai, M.C., Lu, D.W., and Chen, J.T. (2018). Glucosamine-Induced Autophagy through AMPK(-)mTOR Pathway Attenuates Lipofuscin-Like Autofluorescence in Human Retinal Pigment Epithelial Cells In Vitro. *Int J Mol Sci* 19(5). doi: 10.3390/ijms19051416.

Cho, M.I., and Garant, P.R. (2000). Development and general structure of the

periodontium. *Periodontol 2000* 24, 9-27. doi: 10.1034/j.1600-0757.2000.2240102.x.

Choung, H.W., Lee, D.S., Lee, J.H., Shon, W.J., Lee, J.H., Ku, Y., et al. (2016). Tertiary Dentin Formation after Indirect Pulp Capping Using Protein CPNE7. *J Dent Res* 95(8), 906-912. doi: 10.1177/0022034516639919.

Couve, E. (1986). Ultrastructural changes during the life cycle of human odontoblasts. *Arch Oral Biol* 31(10), 643-651. doi: 10.1016/0003-9969(86)90093-2.

Couve, E., Osorio, R., and Schmachtenberg, O. (2013). The amazing odontoblast: activity, autophagy, and aging. *J Dent Res* 92(9), 765-772. doi: 10.1177/0022034513495874.

Craig, R.G., and Peyton, F.A. (1958). Elastic and mechanical properties of human dentin. *J Dent Res* 37(4), 710-718. doi: 10.1177/00220345580370041801.

Crawley, O., and Grill, B. (2021). Autophagy in axonal and presynaptic development. *Curr Opin Neurobiol* 69, 139-148. doi: 10.1016/j.conb.2021.03.011.

D.McKee, J.S.M. (2000). Molecular and cellular biology of alveolar bone. *Periodontology 2000* 24, 99-126.

Depew, M.J., Liu, J.K., Long, J.E., Presley, R., Meneses, J.J., Pedersen, R.A., et al. (1999). Dlx5 regulates regional development of the branchial arches and sensory capsules. *Development* 126(17), 3831-3846.

Duque, C., Hebling, J., Smith, A.J., Giro, E.M., Oliveira, M.F., and de Souza Costa, C.A. (2006). Reactionary dentinogenesis after applying restorative materials and bioactive dentin matrix molecules as liners in deep cavities prepared in nonhuman primate teeth. *J Oral Rehabil* 33(6), 452-461. doi: 10.1111/j.1365-2842.2005.01585.x.

Greenwell, H., Wang, H.L., Kornman, K.S., and Tonetti, M.S. (2019). Biologically guided implant therapy: A diagnostic and therapeutic strategy of conservation and preservation based on periodontal staging and grading. *J Periodontol* 90(5), 441-444. doi: 10.1002/JPER.18-0495.

Huang da, W., Sherman, B.T., and Lempicki, R.A. (2009). Systematic and integrative analysis of large gene lists using DAVID bioinformatics resources. *Nat Protoc* 4(1), 44-57. doi: 10.1038/nprot.2008.211.

Huang, X., Xu, X., Bringas, P., Jr., Hung, Y.P., and Chai, Y. (2010). Smad4-Shh-Nfic signaling cascade-mediated epithelial-mesenchymal interaction is crucial in regulating tooth root development. *J Bone Miner Res* 25(5), 1167-1178. doi: 10.1359/jbmr.091103.

Ichida, F., Nishimura, R., Hata, K., Matsubara, T., Ikeda, F., Hisada, K., et al. (2004). Reciprocal roles of MSX2 in regulation of osteoblast and adipocyte differentiation. *J Biol Chem* 279(32), 34015-34022. doi: 10.1074/jbc.M403621200.

Ishii, M., Han, J., Yen, H.Y., Sucov, H.M., Chai, Y., and Maxson, R.E., Jr. (2005). Combined deficiencies of Msx1 and Msx2 cause impaired patterning and survival of the cranial neural crest. *Development* 132(22), 4937-4950. doi: 10.1242/dev.02072.

Jia, S., Zhou, J., Gao, Y., Baek, J.A., Martin, J.F., Lan, Y., et al. (2013). Roles of Bmp4 during tooth morphogenesis and sequential tooth formation. *Development* 140(2), 423-432. doi: 10.1242/dev.081927.

Jones, C.M., Lyons, K.M., and Hogan, B.L. (1991). Involvement of Bone Morphogenetic Protein-4 (BMP-4) and Vgr-1 in morphogenesis and neurogenesis in the mouse. *Development* 111(2), 531-542.

Jung, H.S., Lee, D.S., Lee, J.H., Park, S.J., Lee, G., Seo, B.M., et al. (2011). Directing the differentiation of human dental follicle cells into cementoblasts and/or osteoblasts by a combination of HERS and pulp cells. *J Mol Histol* 42(3), 227-235. doi: 10.1007/s10735-011-9327-5.

Kim, J.H., Jeon, M., Song, J.S., Lee, J.H., Choi, B.J., Jung, H.S., et al. (2014). Distinctive genetic activity pattern of the human dental pulp between deciduous and permanent teeth. *PLoS One* 9(7), e102893. doi: 10.1371/journal.pone.0102893.

Kim, S.G. (2017). Biological Molecules for the Regeneration of the Pulp-Dentin Complex. *Dent Clin North Am* 61(1), 127-141. doi: 10.1016/j.cden.2016.08.005.

Klingenberg, C.P., Leamy, L.J., Routman, E.J., and Cheverud, J.M. (2001). Genetic architecture of mandible shape in mice: effects of quantitative trait loci analyzed by geometric morphometrics. *Genetics* 157(2), 785-802.

Kronenberg, H.M. (2003). Developmental regulation of the growth plate. *Nature* 423(6937), 332-336. doi: 10.1038/nature01657.

Lallemand, Y., Nicola, M.A., Ramos, C., Bach, A., Clement, C.S., and Robert, B. (2005). Analysis of Msx1; Msx2 double mutants reveals multiple roles for Msx genes in limb development. *Development* 132(13), 3003-3014. doi: 10.1242/dev.01877.

Langmead, B., Trapnell, C., Pop, M., and Salzberg, S.L. (2009). Ultrafast and memory-efficient alignment of short DNA sequences to the human genome. *Genome Biol* 10(3), R25. doi: 10.1186/gb-2009-10-3-r25.

Lanske, B., Amling, M., Neff, L., Guiducci, J., Baron, R., and Kronenberg, H.M. (1999). Ablation of the PTHrP gene or the PTH/PTHrP receptor gene leads to distinct abnormalities in bone development. *J Clin Invest* 104(4), 399-407. doi: 10.1172/JCI6629.

Lee, D.S., Choung, H.W., Kim, H.J., Gronostajski, R.M., Yang, Y.I., Ryoo, H.M., et al. (2014a). NFI-C regulates osteoblast differentiation via control of osterix expression. *Stem Cells* 32(9), 2467-2479. doi: 10.1002/stem.1733.

Lee, D.S., Yoon, W.J., Cho, E.S., Kim, H.J., Gronostajski, R.M., Cho, M.I., et al. (2011a). Crosstalk between nuclear factor I-C and transforming growth factor-beta1 signaling regulates odontoblast differentiation and homeostasis. *PLoS One* 6(12), e29160. doi: 10.1371/journal.pone.0029160.

Lee, H.K., Lee, D.S., Ryoo, H.M., Park, J.T., Park, S.J., Bae, H.S., et al. (2010). The odontogenic ameloblast-associated protein (ODAM) cooperates with RUNX2 and modulates enamel mineralization via regulation of MMP-20. *J Cell Biochem* 111(3), 755-767. doi:

10.1002/jcb.22766.
Lee, J.H., Lee, D.S., Choung, H.W., Shon, W.J., Seo, B.M., Lee, E.H., et al. (2011b). Odontogenic differentiation of human dental pulp stem cells induced by preameloblast-derived factors. *Biomaterials* 32(36), 9696-9706. doi: 10.1016/j.biomaterials.2011.09.007.
Lee, K., Kim, H., and Jeong, D. (2014b). Microtubule stabilization attenuates vascular calcification through the inhibition of osteogenic signaling and matrix vesicle release. *Biochem Biophys Res Commun* 451(3), 436-441. doi: 10.1016/j.bbrc.2014.08.007.
Lee, S.K., Kim, Y.S., Lim, C.Y., and Chi, J.G. (1992). Prenatal growth pattern of the human maxilla. *Acta Anat (Basel)* 145(1), 1-10. doi: 10.1159/000147334.
Lee, Y.S., Park, Y.H., Lee, D.S., Seo, Y.M., Lee, J.H., Park, J.H., et al. (2020). Tubular Dentin Regeneration Using a CPNE7-Derived Functional Peptide. *Materials* 13(20). doi: 10.3390/ma13204618.
Li, W.W., Wang, H.J., Tan, Y.Z., Wang, Y.L., Yu, S.N., and Li, Z.H. (2021). Reducing lipofuscin accumulation and cardiomyocytic senescence of aging heart by enhancing autophagy. *Exp Cell Res* 403(1), 112585. doi: 10.1016/j.yexcr.2021.112585.
Liu, W., Selever, J., Murali, D., Sun, X., Brugger, S.M., Ma, L., et al. (2005). Threshold-specific requirements for Bmp4 in mandibular development. *Dev Biol* 283(2), 282-293. doi: 10.1016/j.ydbio.2005.04.019.
Long, F., and Ornitz, D.M. (2013). Development of the endochondral skeleton. *Cold Spring Harb Perspect Biol* 5(1), a008334. doi: 10.1101/cshperspect.a008334.
Lumsden, A.G. (1988). Spatial organization of the epithelium and the role of neural crest cells in the initiation of the mammalian tooth germ. *Development* 103 Suppl, 155-169.
Lungova, V., Radlanski, R.J., Tucker, A.S., Renz, H., Misek, I., and Matalova, E. (2011). Tooth-bone morphogenesis during postnatal stages of mouse first molar development. *J Anat* 218(6), 699-716. doi: 10.1111/j.1469-7580.2011.01367.x.
Maatouk, D.M., Choi, K.S., Bouldin, C.M., and Harfe, B.D. (2009). In the limb AER Bmp2 and Bmp4 are required for dorsal-ventral patterning and interdigital cell death but not limb outgrowth. *Dev Biol* 327(2), 516-523. doi: 10.1016/j.ydbio.2009.01.004.
Marshall, G.W., Jr. (1993). Dentin: microstructure and characterization. *Quintessence Int* 24(9), 606-617.
Martinez-Cisuelo, V., Gomez, J., Garcia-Junceda, I., Naudi, A., Cabre, R., Mota-Martorell, N., et al. (2016). Rapamycin reverses age-related increases in mitochondrial ROS production at complex I, oxidative stress, accumulation of mtDNA fragments inside nuclear DNA, and lipofuscin level, and increases autophagy, in the liver of middle-aged mice. *Exp Gerontol* 83, 130-138. doi: 10.1016/j.exger.2016.08.002.
Metzger, C.E., Brezicha, J.E., Elizondo, J.P., Narayanan, S.A., Hogan, H.A., and Bloomfield, S.A. (2017). Differential responses of mechanosensitive osteocyte proteins in fore- and hindlimbs of

hindlimb-unloaded rats. *Bone* 105, 26-34. doi: 10.1016/j.bone.2017.08.002.
Miyazaki, T., Baba, T.T., Mori, M., Moriishi, T., and Komori, T. (2015). Microtubule-associated protein tau (Mapt) is expressed in terminally differentiated odontoblasts and severely down-regulated in morphologically disturbed odontoblasts of Runx2 transgenic mice. *Cell Tissue Res* 361(2), 457-466. doi: 10.1007/s00441-015-2135-6.
Mizushima, N. (2007). Autophagy: process and function. *Genes Dev* 21(22), 2861-2873. doi: 10.1101/gad.1599207.
Morita, T., and Sobue, K. (2009). Specification of neuronal polarity regulated by local translation of CRMP2 and Tau via the mTOR-p70S6K pathway. *J Biol Chem* 284(40), 27734-27745. doi: 10.1074/jbc.M109.008177.
Mundlos, S., and Olsen, B.R. (1997). Heritable diseases of the skeleton. Part I: Molecular insights into skeletal development-transcription factors and signaling pathways. *FASEB J* 11(2), 125-132. doi: 10.1096/fasebj.11.2.9039954.
Nanci, A. (2017). *Ten Cate's oral histology-e-book: development, structure, and function.* Elsevier Health Sciences.
Narita, M., Young, A.R., Arakawa, S., Samarajiwa, S.A., Nakashima, T., Yoshida, S., et al. (2011). Spatial coupling of mTOR and autophagy augments secretory phenotypes. *Science* 332(6032), 966-970. doi: 10.1126/science.1205407.
Naveh, G.R., Lev-Tov Chattah, N., Zaslansky, P., Shahar, R., and Weiner, S. (2012). Tooth-PDL-bone complex: response to compressive loads encountered during mastication - a review. *Arch Oral Biol* 57(12), 1575-1584. doi: 10.1016/j.archoralbio.2012.07.006.
Nelms, B.L., and Labosky, P.A. (2010). in *Transcriptional Control of Neural Crest Development*. (San Rafael (CA)).
Nicolatou-Galitis, O., Schiodt, M., Mendes, R.A., Ripamonti, C., Hope, S., Drudge-Coates, L., et al. (2019). Medication-related osteonecrosis of the jaw: definition and best practice for prevention, diagnosis, and treatment. *Oral Surg Oral Med Oral Pathol Oral Radiol* 127(2), 117-135. doi: 10.1016/j.oooo.2018.09.008.
Nishikawa, S., and Kitamura, H. (1987). Microtubules, intermediate filaments, and actin filaments in the odontoblast of rat incisor. *Anat Rec* 219(2), 144-151. doi: 10.1002/ar.1092190206.
Niswander, L., and Martin, G.R. (1993). FGF-4 and BMP-2 have opposite effects on limb growth. *Nature* 361(6407), 68-71. doi: 10.1038/361068a0.
Oh, H.J., Choung, H.W., Lee, H.K., Park, S.J., Lee, J.H., Lee, D.S., et al. (2015). CPNE7, a preameloblast-derived factor, regulates odontoblastic differentiation of mesenchymal stem cells. *Biomaterials* 37, 208-217. doi: 10.1016/j.biomaterials.2014.10.016.
Papapanou, P.N., Sanz, M., Buduneli, N., Dietrich, T., Feres, M., Fine, D.H., et al. (2018). Periodontitis: Consensus report of workgroup 2 of the 2017 World Workshop on the Classification of Periodontal and Peri-Implant Diseases and Conditions. *J Periodontol* 89 Suppl 1, S173-

S182. doi: 10.1002/JPER.17-0721.
Park, Y.H., Lee, Y.S., Park, J.S., Kim, S.H., Bae, H.S., and Park, J.C. (2019). Expression of CPNE7 during mouse dentinogenesis. *J Mol Histol* 50(3), 179-188. doi: 10.1007/s10735-019-09816-0.
Park, Y.H., Lee, Y.S., Seo, Y.M., Seo, H., Park, J.S., Bae, H.S., et al. (2020). Midkine Promotes Odontoblast-like Differentiation and Tertiary Dentin Formation. *J Dent Res* 99(9), 1082-1091. doi: 10.1177/0022034520925427.
Rabinowitz, J.D., and White, E. (2010). Autophagy and metabolism. *Science* 330(6009), 1344-1348. doi: 10.1126/science.1193497.
Rezzani, R., Stacchiotti, A., and Rodella, L.F. (2012). Morphological and biochemical studies on aging and autophagy. *Ageing Res Rev* 11(1), 10-31. doi: 10.1016/j.arr.2011.09.001.
Ribatti, D., and Santoiemma, M. (2014). Epithelial-mesenchymal interactions: a fundamental Developmental Biology mechanism. *Int J Dev Biol* 58(5), 303-306. doi: 10.1387/ijdb.140143dr.
Robledo, R.F., Rajan, L., Li, X., and Lufkin, T. (2002). The Dlx5 and Dlx6 homeobox genes are essential for craniofacial, axial, and appendicular skeletal development. *Genes Dev* 16(9), 1089-1101. doi: 10.1101/gad.988402.
Rosella, D., Papi, P., Giardino, R., Cicalini, E., Piccoli, L., and Pompa, G. (2016). Medication-related osteonecrosis of the jaw: Clinical and practical guidelines. *J Int Soc Prev Community Dent* 6(2), 97-104. doi: 10.4103/2231-0762.178742.
Rubinsztein, D.C., Marino, G., and Kroemer, G. (2011). Autophagy and aging. *Cell* 146(5), 682-695. doi: 10.1016/j.cell.2011.07.030.
Satokata, I., and Maas, R. (1994). Msx1 deficient mice exhibit cleft palate and abnormalities of craniofacial and tooth development. *Nat Genet* 6(4), 348-356. doi: 10.1038/ng0494-348.
Scott, R.C., Schuldiner, O., and Neufeld, T.P. (2004). Role and regulation of starvation-induced autophagy in the Drosophila fat body. *Dev Cell* 7(2), 167-178. doi: 10.1016/j.devcel.2004.07.009.
Seo, Y.M., Park, S.J., Lee, H.K., and Park, J.C. (2017). Copine-7 binds to the cell surface receptor, nucleolin, and regulates ciliogenesis and Dspp expression during odontoblast differentiation. *Sci Rep* 7(1), 11283. doi: 10.1038/s41598-017-11641-y.
Silva, B.S.E., Fagundes, N.C.F., Nogueira, B.C.L., Valladares, J.N., Normando, D., and Lima, R.R. (2017). Epithelial rests of Malassez: from latent cells to active participation in orthodontic movement. *Dental Press J Orthod* 22(3), 119-125. doi: 10.1590/2177-6709.22.3.119-125.sar.
Sodek, J., and McKee, M.D. (2000). Molecular and cellular biology of alveolar bone. *Periodontol 2000* 24, 99-126. doi: 10.1034/j.1600-0757.2000.2240106.x.
Steele-Perkins, G., Butz, K.G., Lyons, G.E., Zeichner-David, M., Kim, H.J., Cho, M.I., et al. (2003). Essential role for NFI-C/CTF transcription-replication factor in tooth root development. *Mol Cell Biol* 23(3), 1075-1084. doi: 10.1128/mcb.23.3.1075-1084.2003.
Tanida, I., Ueno, T., and Kominami, E. (2004). LC3 conjugation system in

mammalian autophagy. *Int J Biochem Cell Biol* 36(12), 2503-2518. doi: 10.1016/j.biocel.2004.05.009.
Tanida, I., Ueno, T., and Kominami, E. (2008). LC3 and Autophagy. *Methods Mol Biol* 445, 77-88. doi: 10.1007/978-1-59745-157-4_4.
Terman, A., and Brunk, U.T. (2004). Lipofuscin. *Int J Biochem Cell Biol* 36(8), 1400-1404. doi: 10.1016/j.biocel.2003.08.009.
Terman, A., Kurz, T., Navratil, M., Arriaga, E.A., and Brunk, U.T. (2010). Mitochondrial turnover and aging of long-lived postmitotic cells: the mitochondrial-lysosomal axis theory of aging. *Antioxid Redox Signal* 12(4), 503-535. doi: 10.1089/ars.2009.2598.
Thesleff, I., and Mikkola, M. (2002). The role of growth factors in tooth development. *Int Rev Cytol* 217, 93-135.
Thesleff, I., Vaahtokari, A., and Partanen, A.M. (1995). Regulation of organogenesis. Common molecular mechanisms regulating the development of teeth and other organs. *Int J Dev Biol* 39(1), 35-50.
Trapnell, C., Pachter, L., and Salzberg, S.L. (2009). TopHat: discovering splice junctions with RNA-Seq. *Bioinformatics* 25(9), 1105-1111. doi: 10.1093/bioinformatics/btp120.
Trapnell, C., Williams, B.A., Pertea, G., Mortazavi, A., Kwan, G., van Baren, M.J., et al. (2010). Transcript assembly and quantification by RNA-Seq reveals unannotated transcripts and isoform switching during cell differentiation. *Nat Biotechnol* 28(5), 511-515. doi: 10.1038/nbt.1621.
Tsuji, K., Cox, K., Bandyopadhyay, A., Harfe, B.D., Tabin, C.J., and Rosen, V. (2008). BMP4 is dispensable for skeletogenesis and fracture-healing in the limb. *J Bone Joint Surg Am* 90 Suppl 1, 14-18. doi: 10.2106/JBJS.G.01109.
van Nievelt, A.F.H., and Smith, K.K. (2005). To replace or not to replace: the significance of reduced functional tooth replacement in marsupial and placental mammals. *Paleobiology* 31(2), 324-346. doi: Doi 10.1666/0094-8373(2005)031[0324:Trontr]2.0.Co;2.
Weinstock, M., and Leblond, C.P. (1974). Synthesis, migration, and release of precursor collagen by odontoblasts as visualized by radioautography after (3H)proline administration. *J Cell Biol* 60(1), 92-127. doi: 10.1083/jcb.60.1.92.
Yang, J.W., Zhu, L.X., Yuan, G.H., Chen, Y.X., Zhang, L., Zhang, L., et al. (2013). Autophagy appears during the development of the mouse lower first molar. *Histochem Cell Biol* 139(1), 109-118. doi: 10.1007/s00418-012-1016-2.
Zeller, R., Lopez-Rios, J., and Zuniga, A. (2009). Vertebrate limb bud development: moving towards integrative analysis of organogenesis. *Nat Rev Genet* 10(12), 845-858. doi: 10.1038/nrg2681.
Zhang, Z., Song, Y., Zhang, X., Tang, J., Chen, J., and Chen, Y. (2003). Msx1/Bmp4 genetic pathway regulates mammalian alveolar bone formation via induction of Dlx5 and Cbfa1. *Mechanisms of Development* 120(12), 1469-1479. doi: 10.1016/j.mod.2003.09.002.
Zhao, X., Zhang, Z., Song, Y., Zhang, X., Zhang, Y., Hu, Y., et al. (2000). Transgenically ectopic expression of Bmp4 to the Msx1 mutant

dental mesenchyme restores downstream gene expression but represses Shh and Bmp2 in the enamel knot of wild type tooth germ. *Mech Dev* 99(1-2), 29-38. doi: 10.1016/s0925-4773(00)00467-6.

ABSTRACT IN KOREAN

성숙한 상아모세포에서 CPNE7 유도-자가포식과 치조골에서 상피간엽상호작용

치아와 치주조직의 발생은 치성 상피와 간엽 간의 순차적인 상호작용을 통해 조절된다. 상피간엽상호작용에는 Copine-7 (CPNE7)과 Bone morphogenetic protein 4 (BMP4)와 같은 다양한 요소들이 작용한다. CPNE7은 상아모세포 분화와 세관 상아질 형성에, BMP4는 사지의 형태 형성과 골 형성에 중요한 역할을 한다고 알려져 있다. 하지만 CPNE7의 생리적 상아질 재생과정이나 BMP4에 대한 치조골과 장골의 다른 반응성의 작용 기전은 아직 명확하게 밝혀지지 않았다.

상아모세포는 수십 년 동안 생체 내에 살아남아 있으며 세포 노화에 따른 지속적인 기능의 감소와 함께 다양한 특징을 나타내는 "유사분열 후 장수하는 세포"로 알려져 있다. 따라서 생리적 상아질 재생을 위해서는 성숙하거나 나이 든 상아모세포의 기능 회복이 필수적이다. 하지만 지금까지 성숙한 상아모세포의 활성을 조절하는 물질은 알려진 바 없다. 이 연구에서는 CPNE7이 자가포식을 유도함으로써 성숙한 상아모세포를 기능적으로 재활성화 시킬 수 있음을 밝혔다. CPNE7은 전상아모세포와 성숙한 상아모세포에서 자가포식의

지표로 널리 알려진 microtubule-associated protein light chain 3 (LC3 II)의 발현과 자가포식소체의 형성을 증가시켰다. 그리고 CPNE7 처리된 성숙한 상아모세포에서 상아질 무기질 침착 지표인 DSP와 DMP-1, 상아질 형성능이 자가포식에 의해 증가했다. 또한 CPNE7에 의해 자가포식이 유도되었을 때 상아모세포 돌기 지표인 NESTIN과 TAU의 발현이 증가했고, 새롭게 활성화된 성숙한 상아모세포의 돌기가 생리적 상아모세포 돌기 형태를 띠었다. 이와 더불어 세포 내에서 세포의 기능을 방해하고 독성을 띠는 노화 색소로 알려진 지방갈색소도 제거했다. 생쥐의 치아 손상모델을 통해 CPNE7은 생체 내에서도 위와 같은 현상들을 동반하며 생리적 상아질을 재생했다. 자가포식 유도제로 가장 잘 알려진 rapamycin 역시 전상아모세포와 성숙한 상아모세포에서 자가포식을 증가시키는 것을 확인했지만 성숙한 상아모세포는 온전히 재활성화 시키지 못했다. 요약하면 위의 결과들은 CPNE7이 성숙한 상아모세포에서 rapamycin과는 다른 방법으로 자가포식을 유도함으로써 상아질 형성과 상아모세포 돌기 연장, 지방갈색소 제거 능력을 복구시킴을 나타낸다.

치조골은 주어지는 자극의 방향에 맞춰 치아를 재배치 함으로써 치아와 치주조직 유지에 중요한 역할을 한다. 그리고 여타의 뼈들과는 달리 치조골은 외부의 물리적 또는 약리적 자극에 대해 다른 반응성을 나타낸다. 특히 장골과 치조골은 근본적인 차이를 지니는데, 이는 발생학적 기원과 상피간엽상호작용이 다르다는 것이다. 이 연구에서는

이러한 근본적인 차이가 치조골과 장골의 서로 다른 반응성을 나타낼 수 있음을 밝혔다. 이를 확인하기 위해서 생쥐의 치조골과 장골의 세포를 일차배양했다. 치조골과 장골에서 얻은 세포들은 형태나 증식률에서는 비슷한 특징을 보였지만 신경능선, 상피간엽상호작용 연관된 유전자의 발현과 무기질 침착능은 다르게 나타났다. 게다가 두 세포의 전사체 프로파일 또한 골 형성, 신경능선, 상피간엽상호작용 연관된 유전자들에서 다른 발현 양상을 보였으며, 그러한 유전자들의 대부분은 골 분화 과정 동안에도 발현 양상에 차이를 보였다. 상피간엽상호작용 연관 단백질 중 BMP4가 골 형성 연관 유전자들과 Msx2, Dlx5, Bmp2의 발현을 장골보다 치조골 유래 세포에서 더 많이 증가시키는 것을 확인했다. 이러한 양상은 골 분화 과정 동안 더 명확하게 확인됐다. 게다가 BMP4가 처리된 치조골 유래 세포는 장골 유래 세포보다 생체 내에서 더 많은 뼈를 형성했다. 이번 연구에서 이러한 발견은 상피간엽상호작용이 치조골과 장골에서 유전자를 다르게 조절함으로써 이에 대한 반응성 역시 다르게 나타남을 보여준다.

총괄해서 보면 이 연구들은 성숙한 상아모세포를 재활성화 시킴으로써 생리적 상아질을 재생하는 CPNE7과 상피간엽상호작용 연관 인자이며 치조골 특이적인 골 형성능을 보이는 BMP4의 작용 기전을 제공한다. 이는 치아와 치조골 손상을 표적으로 하는 CPNE7과 BMP4의 임상적 적용 가능성을 시사한다.

주요어: 상피간엽상호작용, copine-7, BMP4, 자가포식, 재활성화, 반응성
학 번: 2015-22088